

High resolution Holocene paleomagnetic secular variation records from Bay of Bengal

**Usapkar, A¹., Dewangan, P*¹., Badesab, F.¹, Mazumdar, A.¹,
Ramprasad, T.¹, Krishna, K.S.¹, Basavaiah, N.²**

¹CSIR-National Institute of Oceanography, Dona Paula, Goa, India – 403004

²Indian Institute of Geomagnetism (IIG), Panvel, Navi Mumbai, India –410218

* corresponding author: pdewangan@nio.org

Abstract

We present high resolution paleosecular variation (PSV) records up to 8 cal. kyr BP from three piston cores, MD161/8, MD161/11 and MD161/13 acquired in the Krishna-Godavari (KG) basin, Bay of Bengal. During the Holocene period, high sedimentation rates are recorded at MD161/8 (38.8 – 248.3 cm/kyr), MD161/11 (137-336 cm/ky) and MD161/13 (~573 cm/kyr). Rock magnetic data analysis suggests that the remanence signal is carried by titanomagnetite/ titanohematite grains in stable single domain (SSD) / pseudo single domain (PSD) state. The PSV records of MD161/11 and MD161/13 show good correlation in the uppermost sediments despite significant variation in the sedimentation rates; however, poor correlation of PSV records is observed for the core MD161/8 probably due to local effects. Paleoinclination records of MD161/8, MD161/11 and MD161/13 show a low between ~2.4-2.0 cal. kyr BP, an increase between 2.0-1.4 cal. kyr BP and a decrease towards the present. To varying degrees these trends can be observed in the other Asian PSV records of Shuangchiling (SCL) and Biwa lakes. However, the magnitude of the observed inclination anomaly in KG basin is higher (~40°) compared to those reported from SCL (~25°) and Biwa (~10°) lakes. Paleodeclination records of MD161/11 and MD161/13 show a decline between ~4.0-2.9 cal. kyr BP, an increase between 2.9-2.1 cal. kyr BP, a substantial decrease between ~2.1- 1.0 cal. kyr BP and an increase towards the present. Similar trends can be observed in the other Asian PSV records of SCL and Biwa lakes with a minor age offset of 0.2 to 0.5 kyr. The available models CALS7k.2 and CALS10k.1 are evaluated for their capability in predicting the inclination and declination anomalies from the Asian regions. The CALS7k.2 model can predict most of the inclination anomalies while the CALS10k.1 is unable to predict many of them. The CALS7k.2 model shows that the observed inclination anomalies can be attributed to the presence of a strong non-axial dipolar magnetic field over the Bay of Bengal. More PSV records need to be constructed to better understand the anomalous non-axial dipolar field over the Bay of Bengal.

1. Introduction

Paleomagnetic studies are being carried out worldwide to establish high resolution paleosecular variation (PSV) records that can be used to correlate regional stratigraphies (Turner and Thompson 1981, 1982; Hagstrum and Champion 2002; St-Onge et al., 2003; Snowball et al., 2007; Barletta et al., 2010a, 2010b, Snowball and Sandgren 2002; Lund and Banerjee 1985; Verosub et al., 1986; Creer and Tucholka 1982; Lisé-Pronovost 2009; Roberts et al., 2013) and to understand the geodynamo processes responsible for the Earth's magnetic field (Merril et al., 1996; McFadden and Merrill, 1995). Historical observation of PSV data is available only for the last 400 years (Jackson et al., 2000). Prior to direct observations, the variation of Earth's magnetic field on millennial scale can be reconstructed using archeological materials and volcanic rocks as well as from rapidly deposited, well-dated lake/marine sedimentary sequences (e.g., Stockhausen, 1998; Ali et al., 1999; Frank et al., 2002; Vigliotti, 2006; Irurzun et al., 2006, 2008; Snowball et al., 2007). Most of the PSV records documenting the Holocene are from Europe (Vigliotti et al., 2006; Sagnotti et al., 2011; Stockhausen, 1998; Opdyke et al., 1972; Thompson 1975; Turner and Thompson 1981), North America (Creer and Tucholka 1982; Lund and Banerjee 1985; Verosub et al., 1986; Hanna and Verosub 1989; Sprowl and Banerjee, 1989; King 1983), central Asia (Gomez-Páccard, 2012; Péck et al., 1996; Nurgaliev et al., 1996, Nourgaliev 2003) and South East Asia (Ali et al., 1999; Hyodo et al., 1999; Yang et al., 2009, 2013; Zheng et al., 2014). The scarcity of Holocene PSV records within 20° of the Equator limits our ability to understand time and space variability of the Earth's magnetic field and related geodynamo processes. Moreover, such high resolution PSV records are not available from the northern Indian Ocean. Therefore, we attempt to establish the high resolution and continuous PSV records from the high sedimentation regions of Krishna Godavari (KG) basin, Bay of Bengal, using three Calypso piston cores MD161/8 (~30 m, water depth= 1033 m, Lat=15° 51.8624'N, Lon=81° 50.0692'E) , MD161/11 (~28m, water depth= 1007 m, Lat= 15° 54.0217'N, Lon=81° 48.1366'E) and MD161/13 (~29 m, water depth=647 m, Lat=16° 01.9684'N, Lon=81° 42.7909'E) acquired onboard *M/V Marion Dufresne* in 2007. The PSV records are evaluated for their potential to act as a reliable tool for magnetic stratigraphy as well as to understand the geodynamo processes manifested over the Bay of Bengal.

2. Geology of the study area

Krishna Godavari (KG) basin is a petroliferous basin in the Bay of Bengal. It is a pericratonic rift basin formed due to the breakup of Gondwanaland around 130 Ma years ago (Sastri et al., 1981;

Rao, 2001; Powell et al., 1988; Scotese et al., 1988; Ramana et al., 1994). It encompasses an area of 28,000 sq. km onshore and 145,000 sq. km offshore (Ojha and Dubey, 2006) and stretches from the Ongole in south to the Vishakhapatnam in north. Thickness of onshore sediments varies between ~ 3 and 5 km which increases to ~8 km in offshore region (Prabhakar and Zutshi 1993; Bastia 2007). The thick sediment strata largely composed of montmorillonite clay (Rao, 1991) are brought by Krishna and Godavari rivers and their tributaries which originate in the Western Ghats and run over the provenance of Deccan trap basalts. Environmental magnetic studies by Sangode et al., (2007) showed higher magnetic susceptibility values in Godavari basin in comparison with those from other basins in Indian subcontinent.

The studied cores (MD161/8, MD161/11 and MD161/13) were acquired from the continental slope region of the KG basin (Fig. 1). Sedimentological studies show that the grain size of the sediment is predominantly clay (~70 %) and silt (~30 %) with traces of sand fraction (NIO, 2005). Further, X-Ray analysis of clay minerals suggests the presence of montmorillonite clay with traces of illite and kaolinite. The dominant detrital magnetic minerals, as evident from the SEM-EDS analysis of the magnetic extracts, are titanomagnetite and titanohematite with varying amount of Ti/Fe ratio from 0.2 to 0.45 (Dewangan et al., 2013, Usapkar et al., 2014). The presence of sub-surface hydrates is confirmed in the KG basin from drilling/coring activities during NGHP Expedition 01 (Kumar et al., 2014). Geophysical signatures associated with fluid/gas migration have also been documented in KG basin indicating migration of methane gas through the sediment (Ramana et al., 2009; Dewangan et al., 2010; Ramprasad et al., 2011). Geochemical signatures related to a paleo-cold seep activity are also reported in KG offshore basin (Mazumdar et al., 2009). The geochemical processes such as anaerobic oxidation of methane (AOM) may significantly alter the magnetic minerals and affect the magnetic measurements. The detailed rock magnetic measurements of the core MD161/8 reveal dissolution of magnetic minerals and authigenic growth of secondary iron sulfides below 7 m related to methane seep (Dewangan et al., 2013), and such diagenetically altered sediments are not considered in the present study.

3. Methodology

The cores MD161/8, MD161/11 and MD161/13 collected primarily for gas hydrate studies are used to reconstruct the PSV records in the Bay of Bengal. After retrieval, the core was split in two halves and was cut in to sections of length 1 to 1.5 m. About 20 cm sub-sampling was carried out immediately from each section for micro-biology and pore-water chemistry studies related to gas hydrates. Cores (MD161/8 and MD161/13) were subsampled at a resolution of 2 cm using 7 cm³

cylindrical vials for paleomagnetic investigations. The core MD161/11 was subsampled eight years later at a resolution of 5 cm to substantiate the results obtained from MD161/8 and MD161/13 cores. The orientation of the sample was fixed with respect to a reference line pre-marked along the length of the core liner. All remanent magnetisation values were measured on the discrete samples using a Molspin fluxgate spinner magnetometer. Paleomagnetic measurements on the sediment samples from MD161/8 core were carried out at the environmental magnetic laboratory, Indian Institute of Geomagnetism (IIGM), Panvel, India; whereas paleomagnetic measurements on the samples from MD161/11 and MD161/13 cores were carried out at paleomagnetic laboratory, National Institute of Oceanography (NIO), Goa, India. The samples from MD161/8 were progressively demagnetised using an alternating field (AF)-Demagnetiser from 0 to 100 mT in steps of 10 mT, and characteristic remanent magnetisation (ChRM), i.e., paleomagnetic inclination, declination and intensity as well as the maximum angle of deviation (MAD) were calculated by using Principal Component Analysis (PCA: Kirschvink, 1980). In case of MD161/13, one pilot sample per section (1.5 m) was progressively AF-Demagnetised from 0 to 40 mT in steps of 5 mT and then to 100 mT in steps of 10 mT. The analysis of demagnetisation results of pilot samples from MD161/13 suggests that the viscous component of NRM can be removed by applying 15 mT demagnetisation field. Therefore, the remaining samples of MD161/13 were demagnetised at 15 mT to obtain the paleomagnetic inclination, declination and intensity records. The samples from MD161/11 were progressively AF-Demagnetised from 0 to 50 mT in steps of 10 mT, and ChRM as well as MAD were calculated using PCA analysis. The paleointensity record for the cores is obtained by normalizing the respective NRM values by susceptibility and is shown in Figure 4C.

High resolution rock magnetic data of the sediment core MD161/8 have been reported by Dewangan et al. (2013). Following a similar methodology, rock magnetic measurements were carried out on wet samples at a resolution of 10 cm for MD161/13 core. Magnetic susceptibility measurements were performed using Bartington MS2B dual frequency susceptibility meter. Susceptibility was measured at two different frequencies $\chi_{LF} = 0.47$ kHz and $\chi_{HF} = 4.7$ kHz and the frequency dependent susceptibility was computed as $\chi_{fd}\% = (\chi_{LF} - \chi_{HF}) / \chi_{LF} \times 100$. Anhyseric remanent magnetisation (ARM) was imparted using 100 mT AF field superimposed with a fixed DC bias field of 50 μ T. Susceptibility of ARM is calculated as mass normalized ARM divided by the DC bias field. Isothermal remanent magnetisation (IRM) of 1 T in forward direction and -20 mT, -30 mT, -100 mT and -300 mT in backward direction were imparted to the sediment samples using a MMP10 pulse magnetiser. Mass-normalized IRM acquired with a peak field of 1T is assumed to be the saturation isothermal remanent magnetization (SIRM). S-ratio is computed using formula (S-ratio = IRM.

$_{300\text{mT}}/IRM_{1T}$: Thompson and Oldfield, 1986; Bloemendal et al., 1988). Soft-IRM and Hard-IRM (HIRM) were computed using formulae [$\text{Soft-IRM} = (IRM_{1T} + IRM_{300\text{mT}}) / 2$] and [$\text{HIRM} = (IRM_{1T} + IRM_{300\text{mT}}) / 2$] (Liu et al., 2007).

4. Results

4.1 Paleomagnetic record

The AF-demagnetisation results of NRM were analysed using Zijderveld vector end point diagrams (Zijderveld, 1967). The Zijderveld plots of some of the samples from the MD161/8 (Fig. 2A), MD161/11 (Fig. 2B) and MD161/13 (Fig. 2C) show that the data points (≥ 20 mT) lie on a straight line trending towards the origin indicating the presence of stable ChRM. The inclination, declination and intensity records of MD161/8, MD161/11 and MD161/13 are shown in Figure 3A, 3B and 3C, respectively and the values are listed in Table-1. The sedimentation rates, as estimated from radiocarbon ages, are very high in the KG basin during Holocene and show significant temporal and spatial variations (Mazumdar et al., 2012). The topmost sediments (< 4 mbsf) of core MD161/8 show a very high sedimentation rate of 248 cm/kyr which decreases to 86.7 cm/kyr between 4 and 7 mbsf (Mazumdar et al., 2009). The uppermost 7 mbsf of MD161/8 covers the late Holocene period up to 8 cal. kyr BP. The PSV records of MD161/8 below 7 mbsf are excluded from the present study due to diagenesis of magnetic minerals owing to sulfidisation (Dewangan et al., 2013). The average sedimentation rate of MD161/13 is extremely high around 573 cm/kyr, and the top 22 m extends up to 4 cal. kyr BP (Mazumdar et al., 2012). A rapid increase in sedimentation rates below 22 mbsf possibly relates to reported mass transport deposits (MTD; Mazumdar et al., 2012); therefore, the magnetic records of MD161/13 below 22 m are excluded from the present study. The uppermost 8 mbsf of MD161/11 shows a sedimentation rate of 336 cm/kyr which decreases to 137 cm/kyr between ~ 8 and 13 mbsf. Rapid sedimentation is observed below 13 mbsf possibly associated with MTDs, therefore the PSV records below 13 mbsf are not used in the present study. The top 1.5 m of the sediment cores was highly disturbed due to piston coring, and is not used for NRM studies. Due to the vast differences in sedimentation rate, the PSV records are expressed in terms of age rather than depth to facilitate better comparison between the inclination (Fig. 4A), declination (Fig. 4B) and paleointensity (Fig. 4C) of cores MD161/8, MD161/11 and MD161/13.

In spite of the differences in the sedimentation rates, paleoinclination records of MD161/8, MD161/11 and MD161/13 show broad similarity in variation pattern (Fig. 4A). The paleoinclination records show significant fluctuations between -20° and 20° (approx.) for the uppermost sediment ($<$

4 cal. kyr BP) in contrast to the expected axial dipole field inclination of 30° at these locations. The core MD161/13 shows significantly low inclination values as compared to the expected value at 0.6, 2.2 and 3.8 cal. kyr BP, while low inclination values are observed at 2.0 and 5.8 cal. kyr BP for MD161/8. Similar low inclination values are also observed at ~ 2 , 4.3 and 7 cal. kyr BP for MD161/11. Higher values of inclination ($> 30^\circ$) are observed at 1.4 cal. kyr BP for cores MD161/11, MD161/13 and possibly for core MD161/8.

The paleodeclination profiles of MD161/8, MD161/11 and MD161/13 represent relative variations in declination as the cores were not oriented with respect to geographic north. The relative paleodeclination of MD161/8 is obtained from ChRM declination by subtracting an arbitrary constant of 180° so that it fluctuates around zero. No correction was applied for the relative paleodeclination of MD161/13. An arbitrary constant of 250° was subtracted from paleodeclination values of MD161/11. The relative paleodeclination of MD161/11 and MD161/13 shows a broad similarity pattern from 5.4 cal. kyr BP to Recent (Fig. 4B). An increase in declination is observed between 5.4 and ~ 4.3 cal. kyr BP in MD161/11 core. A gradual decrease in declination is observed between 4.3 and 2.9 cal. kyr BP in MD161/11 and MD161/13 cores. The declination further increases with minor oscillations between 2.9 and ~ 2.0 cal. kyr BP. The sharp decrease of declination by about 100° is observed from 2.0 to 1.0 cal. kyr BP. Further, an increasing trend is observed towards Recent in core MD161/13. The declination profile of MD161/8 shows essentially no trend over most of the time interval, however it depicts a decline in paleodeclination between 2 and ~ 1.4 cal. kyr BP as observed in cores MD161/11 and MD161/13.

An increase in paleointensity is observed between ~ 6 and ~ 4 cal. kyr BP in MD161/8 and MD161/11 cores. A gradual decrease is observed between 4 and 3 cal. kyr BP in MD161/11 and MD161/8 cores, while the trend is reverse in MD161/13 core. Further, a constant trend with minor undulations is observed towards Recent in all the cores. Overall, the paleointensity records of MD161/8, MD161/11 and MD161/13 are poorly correlated and probably reflect the variation in the concentration, grain size and mineralogy of the magnetic minerals. Therefore, the paleointensity records are not utilised for interpretation in the present study.

4.2 **Rock magnetism:** Magnetic mineral concentration and magnetic granulometry

The detailed rock magnetic parameters for the core MD161/8 have been reported by Dewangan et al. (2013). In the present study, the rock magnetic studies related to the core MD161/13 was carried out and the results are presented in Table 2. The average values and standard deviation of different rock

magnetic parameters for MD161/13 and MD161/8 cores are listed in Table 3. The magnetic parameters χ , ARM and SIRM are mainly related to the concentration of magnetic minerals while ARM is sensitive to single domain (SD) and pseudo-single domain (PSD) grains. The χ_{LF} and SIRM are also sensitive to coarser grain sizes of magnetic minerals mainly in the multidomain (MD) state (Dunlop 1973; Bailey and Dunlop 1983; Thompson and Oldfield, 1986). In general, a trend of down core decrease is observed for the parameters χ_{LF} , χ_{ARM} , and SIRM suggesting gradual reduction in the abundance of magnetic minerals (Fig. 5A-C). A minor increase in χ_{LF} and SIRM is observed between 2.5 and 3.5 cal. kyr BP. A similar increase is also seen in χ_{ARM} over the same time interval. This reflects the possible occurrence of relatively higher proportion of finer magnetic grains (SSD/PSD) in this interval.

The interparametric ratios ARM/SIRM, SIRM/ χ_{LF} and $\chi_{fd}\%$ are regarded as potential magneto-granulometric indicators while S-ratio depends on the magnetic minerals. The soft- and hard-IRM values reflect the abundance of soft and hard magnetic minerals, respectively (Banerjee et al., 1981; Maher, 1988; Oldfield, 1994). The $\chi_{fd}\%$ values for the majority of the samples are $< 5\%$ indicating minor contributions from superparamagnetic (SP) particles (Fig. 6A). The ARM/SIRM and $\chi_{fd}\%$ show gradual downcore increase from present to 2.8 cal. kyr BP indicating the relative increase in the abundance of fine grained magnetic minerals (Fig. 6 A, B). Further downcore (> 2.8 cal. kyr BP), a decrease in ARM/SIRM and $\chi_{fd}\%$ as well as the increase in SIRM/ χ_{LF} (Fig. 6C) can be attributed to the coarsening of magnetic grains. The S-ratio is close to 0.95 indicating the dominance of soft magnetic minerals (Fig. 6D). Soft-IRM and hard-IRM values (Fig. 6E and Fig. 6F) show a gradual decreasing trend downcore; however, a minor increase in hard-IRM values is observed between 3 and 3.2 cal. kyr BP.

5. Discussion

5.1. Assessment of the quality of PSV records: Pros, cons and limits

A good quality high resolution PSV record requires a continuous core from a high sedimentation region. High concentration of unaltered magnetic minerals in a stable single domain (SSD) / pseudo single domain (PSD) state is a pre-requisite for stable remanent magnetisation. High influx of magnetic minerals owing to high sedimentation rates provides an ideal geological environment to construct PSV records. The sedimentation rates (SRs) in the shelf and slope regions of KG basin are high; average SR for core MD161/13 is 573 cm/kyr and the SRs for the upper most 7 m of core MD161/8 range from 86.7 to 248 cm/kyr. A variable sedimentation rate of 336 cm to 137 cm/kyr is

observed for upper 13 m of core MD161/11 (Mazumdar et al., 2012). Previous environmental magnetic studies by Sangode et al. (2007) showed that Godavari basin receives huge concentrations of magnetic minerals from Deccan flood basalts, and possesses high magnetic susceptibility in comparison with other depositional environments from Indian subcontinent. Therefore, the sediment cores retrieved from this basin were investigated to construct high resolution PSV records. The other factors which could also potentially influence the reliability of PSV records are the variability in magnetic mineral concentration, magnetic grain size and mineralogy. Hence these parameters are also studied to assess the reliability of PSV records.

The X-Ray diffraction (XRD) analysis of magnetic extracts suggests that the dominant magnetic mineral is titanomagnetite in the study area (Dewangan et al., 2013; Usapkar et al., 2014). Detailed magnetic measurements are carried out for core MD161/13 to understand the magnetic mineralogy, concentration, grain size and the signatures associated with reductive dissolution of magnetic minerals. The downcore decrease in parameters χ_{LF} , χ_{ARM} and SIRM of MD161/13 (Fig. 5) suggests reduction in the concentration of the magnetic minerals with depth due to sulfidisation (Peketi et al., 2015). The values of χ_{ARM} gradually increase from 4 to 3 cal. kyr BP, thereafter remain almost constant until Recent. High values of χ_{ARM} suggest the presence of magnetic grains in SSD/PSD state which are capable of acquiring stable NRM. The low values of $\chi_{fd}\%$ (Fig. 6A) suggest a minor presence of SP grains. The grain size dependent ratios ARM/SIRM and SIRM/ χ_{LF} (Fig. 6B, C) suggest a uniform SSD/PSD magnetic grain size from 3 cal. kyr BP to present. A gradual down core increase in SIRM/ χ_{LF} ratio (> 2.5 cal. kyr BP) suggests higher abundance of PSD grains as compared to the SSD grains. An abrupt increase in SIRM/ χ_{LF} ratio around 2.5 cal. kyr BP may indicate the presence of SSD greigite (Roberts et al., 1996; Snowball 1997; Walden et al., 1999). The average S-ratio of core MD161/13 is around 0.95 indicating a uniform mixture of titanomagnetite and titanohaematite minerals (Thompson and Oldfield 1986; Bloemendal et al., 1992; St-onge et al., 2003; Heslop 2009). The Soft -IRM and hard-IRM values represent relative concentration of low coercivity titanomagnetite and hard coercivity titanomagnetite and/or titanohematite, respectively.

Similarly, the magnetic parameters (χ_{LF} , χ_{ARM} , SIRM) of core MD161/8 show a decreasing trend for the topmost sediments (< 7 mbsf) owing to the sulfidisation (Dewangan et al., 2013). The downcore decrease in SIRM/ χ_{LF} ratio for the uppermost sediments (< 5 mbsf) suggests a relative downcore increase in the concentration of SSD particles. An abrupt decrease in S-ratio around 5 cal. kyr BP indicates an increase in the abundance of titanohaematite.

The magnetic parameters χ and SIRM relate to the concentration of ferrimagnetic mineral components while S-ratio and HIRM are indicative of magnetic mineralogy. The cross plots between SIRM and χ for MD161/8 (Fig. 7A) and MD161/13 (Fig. 7B) show several different slopes and trends within each data set suggesting downcore variations in composition, grain size and concentration. The details of the rockmagnetic analysis on the studied cores confirm the presence of detrital ferrimagnetic minerals (titanomagnetite) in the SSD/PSD state. Therefore, the cores are suitable for PSV studies. However, the abrupt change in magnetic mineralogy as inferred from the S-ratio should be taken into account while interpreting the PSV records.

5.2 Intrasite reproducibility of PSV records and regional correlation

In order to test the reliability and reproducibility, PSV records of MD161/8, MD161/11 and MD161/13 are compared, and later they are correlated with similar records from the nearby Asian regions Shuangchiling (SCL) Hainan, south east of China (Lat: 19°N, Lon: 110°E; Yang et al., 2009) and Biwa lake (lat: 35°N, Lon: 110°E; Ali et al., 1999), Japan. Smoothed Paleoinclination records of MD161/8 (5 pt average), MD161/11 (5 pt average) and MD161/13 (9 pt average) show broad similarity despite significant variations in the sedimentation rates (Fig. 8A). Paleoinclination records of MD161/8, MD161/11 and MD161/13 show a low between ~2.4-2.0 cal. kyr BP, an increase between 2.0-1.4 cal. kyr BP and a decrease towards the Recent. To varying degrees similar trends in paleoinclination can also be observed in other two Asian records of SCL and Biwa lakes with a minor age offset of 0.2 to 0.5 cal. kyr. The strong low in paleoinclination observed in MD161/8 at 5.8 cal. kyr BP cannot be identified in other records; therefore it may be related to local effects. The inclination anomaly at ~4.3 cal. kyr BP is prominent in core MD161/11, but cannot be identified on MD161/8 core. An increasing trend in core MD161/13 between 4.0-2.4 cal. kyr BP probably relates to 4.3 cal. kyr BP anomaly. This low is also identified in SCL and Biwa lake records with a minor age offset. The magnitude of the inclination anomalies (~40°) as observed in the Bay of Bengal is higher than that of SCL-lake (~25°) and Biwa lake (~10°). It is interesting to note that the magnitude of inclination anomaly appears to be increasing towards the low-latitude regions. The consistency and correlatability in the paleoinclination records on a broader scale among the three Asian regions suggests that the PSV records of Bay of Bengal can be reliable and thus be used to understand the geo-dynamo processes in Bay of Bengal. They can also act as reference curves, and the observed inclination anomalies can be used for site-to-site correlation and for relative dating during Holocene.

Paleodeclination records of MD161/11 and MD161/13 depict a decline between ~4.0-2.9 cal. kyr BP, an increase between 2.9-2.1 cal. kyr BP, a significant decrease between ~2.1- 1.0 cal. kyr BP and

an increase towards the present. In general, the smoothed paleodeclination patterns from 4.0 cal. kyr BP to Recent of MD161/11 and MD161/13 cores in Bay of Bengal are similar to other Asian records of SCL and Biwa lakes (fig. 8B). However, records from the Bay of Bengal show a larger swing in relative paleodeclination as compared to that of SCL and Biwa lakes. An increase in paleodeclination is observed between 5.4 - 4.5 cal. kyr BP for core MD161/11 which matches well with records of SCL and Biwa lakes with a minor age offset. Inconsistent paleodeclination trend is also observed among the Asian cores from 8-5.8 cal. kyr BP which may be attributed to the twisting/turning of the core during piston coring process (Ali et al., 1999). Also, the splitting of the core along the marked reference line may introduce some errors in the observed declination values. It may also happen that the differences in trend may be of geomagnetic origin owing to local effects (Frank et al., 2002).

5.3 Modeling and analysis of the observed inclination anomaly

In order to understand the governing factors for the observed inclination anomaly in the Asian records, the paleoinclination records of Asian records are compared with those computed from the available CALS7k.2 and CALS10k.1b models (Korte et al., 2005; Korte et al., 2011). The model represents time and space variability of paleo-geomagnetic field using spherical harmonics. The coefficients of spherical harmonics are obtained from published PSV records for the past 10 kyr (8000 BC to 1990 AD). The paleoinclination records from CALS7k.2 model at the locations of MD161/8, MD161/11, MD161/13, SCL and Biwa lakes (Fig. 8A) show lower inclination values at 0.4, 2.2, 4.3 and 5.8 cal. kyr BP as compared to the expected value. The observed data at these locations also show similar lows in inclination at 0.6, ~2.2 and 4.3 cal. kyr BP; however, the magnitude of the observed anomalies in Bay of Bengal is stronger. In contrast, the CALS10k.1b model is predicting higher inclination values at 2.2, 4.3 and 5.8 cal. kyr BP which is not supported by the data from the Asian regions.

The non-axial dipolar (NAD) inclination anomaly, defined as the difference between the modeled inclination with all coefficients and that predicted by the axial dipole coefficient, is computed for both CALS7k.2 and CALS10k.1b models at specific time intervals 0.6, 2.2, 4.3 and 5.8 cal. kyr BP (Fig. 9) to understand its effect over the Bay of Bengal. The inclination anomaly due to non-axial dipolar field as predicted by CALS7k.2 model is strongest over the Bay of Bengal at these time intervals (Fig. 9A). The correlation between the observed and modeled data suggests that the observed inclination anomaly may be related to the non-axial dipolar components of the Earth's magnetic field. In contrast, the CALS10k.1b model depicts an opposite trend in the temporal

variation of non-axial dipolar field in the Asian region (Fig. 9B) and is not consistent with the observed data. In fact, the average non-axial dipolar anomaly during the Holocene period shows a negative inclination anomaly over the Asian region from CALS7k.2 model and positive inclination anomaly from CALS10k.1b model (Korte et al., 2011).

The effect of non-axial dipolar field seems to be stronger over the Bay of Bengal as compared to other Asian regions like China or Japan which may explain higher intensity anomalies as observed in the present study. The initial results from KG basin show abnormal behavior of the geomagnetic field over the Bay of Bengal. Therefore, more PSV records from the high sedimentation regions of the Indian Ocean are required to understand the geodynamo processes over Bay of Bengal.

Conclusion

In the present study, PSV records are studied from KG basin, Bay of Bengal, for the past 8 cal. kyr BP. High sedimentation rates and continuous deposits with good age control provide good correlation in both inclination and declination records between the cores MD161/11 and MD161/13. Poor correlation is observed for the core MD161/8 which may be related to local effects. Interestingly, the PSV records from KG basin show a pattern similar to that observed from other Asian sites. Four major paleoinclination anomalies are observed at 0.6, 1.4, 2.2 and 4.3 cal. kyr BP in the Bay of Bengal. The lows in paleoinclination at 0.6, 2.2 and 4.3 cal. kyr BP are also predicted by CALS7k.2 model, but the intensity of the observed anomalies is stronger than that predicted by the model. Further, these inclination anomalies may be related to non-axial dipolar components of the Earth's magnetic field centered over the Bay of Bengal. The PSV record can be used for regional correlation as well as for relative dating of the Holocene sediments.

Acknowledgements

We thank the Director, CSIR-NIO for his support and permission to publish the paper. We also thank the Directors of NIOT and NCAOR, and the Secretary, Ministry of Earth Sciences for providing financial support for sediment coring onboard RV *Marion Dufresne*. The crew and officers of the RV *Marion Dufresne*, scientific and technical staff from NIO, NIOT and NGRI, and students from Goa University are also acknowledged for their support during the acquisition of cores. We would like to thank Daryl Vaz for preparing the final figures and Satyendra Singh Panwar for modeling the geomagnetic field. We like to thank Prof. Akira Hayashida, Drs. M. Ali and Hirokuni Oda for providing data of PSV records of Biwa lake and Prof. Yang Xiaoqiang for sharing the data from SCL lake. We thank the anonymous reviewers for their valuable suggestions which have improved the quality of the manuscript. VNJCT fellowship to Ms. Asha Usapkar is sincerely acknowledged. This is CSIR-NIO contribution no xxx.

References:

1. Ali, M., Oda, H., Hayashida, A., Takemura, K., Torii, M., 1999. Holocene palaeomagnetic secular variation at lake Biwa, central Japan. *Geophysics Journal International* 218–228.
2. Bailey, M.E., Dunlop, D.J., 1983. Alternating field characteristics of pseudo-single-domain (2-14 μm) and multidomain magnetite. *Earth and Planetary Science Letters* 63,335-352.
3. Banerjee, S.K., King, J., Marvin, J., 1981. A rapid method for magnetic granulometry with applications to environmental studies. *Geophysical Research Letters*, 8, 333 - 336.
4. Barletta, F., St-Onge, G., Channell, J.E.T., Rochon, A., 2010a. Dating of Holocene western Canadian Arctic sediments by matching paleomagnetic secular variation to a geomagnetic field model. *Quaternary Science Reviews* 29, 2315–2324.
5. Barletta, F., St-Onge, G., Stoner, J. S., Lajeunesse, P., Locat, J., 2010b. A high-resolution Holocene paleomagnetic secular variation and relative paleointensity stack from eastern Canada. *Earth and Planetary Science Letters* 298(1), 162-174.
6. Bastia, R., 2007. Geologic settings and petroleum systems of India's east coast offshore basins : concepts and applications. Technology Publications, Dehradun, p204.
7. Bloemendal, J., Lamb, B., King, J., 1988. Paleoenvironmental implications of rock-magnetic properties of late Quaternary sediment cores from the eastern equatorial Atlantic. *Paleoceanography* 3, 61–87.
8. Bloemendal, J., King, J.W., Hall, F.R., Doh, S-J., 1992. Rock magnetism of late Neogene and Pleistocene deep-sea sediments: relationship to sediment source, diagenetic processes and sediment lithology. *Journal of Geophysical Research* 97, 4361-4375.
9. Creer, K.M., Tucholka, P., 1982. Construction of type curves of geomagnetic secular variation for dating lake sediments from east central North America. *Canadian Journal of Earth Sciences* 19(6), 1106–1115.
10. Dewangan, P., Ramprasad, T., Ramana, M. V., Mazumdar, A., Desa, M., Badesab, F.K., 2010. Seabed morphology and gas venting features in the continental slope region of Krishna–Godavari basin, Bay of Bengal: implications in gas-hydrate exploration. *Marine and Petroleum Geology* 27, 1628–1641.
11. Dewangan, P., Basavaiah, N., Badesab, F.K., Usapkar, A., Mazumdar, A., Joshi, R., Ramprasad, T., 2013. Diagenesis of magnetic minerals in a gas hydrate/cold seep environment off the Krishna-Godavari basin, Bay of Bengal. *Marine Geology* 340, 57–70.
12. Dunlop D.J., 1973. Superparamagnetic and single-domain threshold sizes in magnetite. *Journal of Geophysical Research* 78, 1780-1793.
13. Frank, U., Nowaczyk, N.R., Negendank, J.F.W., Melles, M., 2002. A paleomagnetic record from Lake Lama , northern Central Siberia. *Physics of the Earth and Planetary Interiors* 133, 3–20.
14. Gómez-Paccard, M., Larrasoña, J.C., Giralt, S., Roberts, A.P., 2012. First paleomagnetic results of mid- to late Holocene sediments from Lake Issyk-Kul (Kyrgyzstan): implications for paleosecular variation in central Asia. *Geochemistry Geophysics Geosystems* 13, Q03019, doi:10.1029/2011GC004015.

15. Hagstrum, J.T., Champion, D.E., 2002. A Holocene paleosecular variation record from ^{14}C -dated volcanic rocks in western North America. *Journal of Geophysical Research: Solid Earth* 107(B1), EPM-8.
16. Hanna, R. L., Verosub, K. L., 1989. A review of lacustrine paleomagnetic records from western North America: 0–40000 years BP. *Physics of the Earth and Planetary Interiors*, 56(1), 76-95.
17. Heslop, D., 2009. On the statistical analysis of the rock magnetic S-ratio. *Geophysical Journal International*, 178(1), 159-161.
18. Hyodo, M., Yoshihara, A., Kashiwaya, K., Okimura, T., Masuzawa, T., Nomura, R., Tanaka, S., Xing, T.B., Qing, L., S., Jian, L.S. 1999. A late Holocene geomagnetic secular variation record from Erhai Lake, southwest China. *Geophysical Journal International*, 136(3), 784-790.
19. Irurzun, M. A., Gogorza, C.S.G., Chaparro, M. A. E., Lirio, J.M., Nuñez, H., Vilas, J.F., Sinito, A. M., 2006. Paleosecular variations recorded by Holocene-Pleistocene sediments from Lake El Trébol (Patagonia, Argentina). *Physics of the Earth Planetary Interiors* 154, 1–17.
20. Irurzun, M. A., Gogorza, C. S. G., Sinito, A. M., Chaparro, M. A. E., Nuñez, H., & Lirio, J. M., 2008. Paleosecular variations 12–20 Kyr as recorded by sediments from Lake Moreno (southern Argentina). *Studia Geophysica et Geodaetica* 52(2), 157-172.
21. Jackson, A., Jonkers, A. R., Walker, M. R., 2000. Four centuries of geomagnetic secular variation from historical records. *Philosophical Transactions of the Royal Society of London A: Mathematical, Physical and Engineering Sciences*, 358(1768), 957-990.
22. King, J.W., 1983. Geomagnetic secular variation curves for northeastern North America for the last 9,000 years BP. Ph.D. thesis, University of Minnesota, Minneapolis.
23. Kirschvink, J. L., 1980. The least-squares line and plane and the analysis of paleomagnetic data. *Geophysical Journal International*, 62, 699–718.
24. Korte M., Constable C. G., 2005. Continuous geomagnetic field models for the past 7 millenia: 2. CALS7K. *Geochemistry Geophysics Geosystems* 6, Q02H16, doi: 10.1029/2004GC000801.
25. Korte, M., Constable, C., Donadini, F., Holme, R., 2011. Reconstructing the Holocene geomagnetic field. *Earth and Planetary Science Letters* 312, 497-505.
26. Kumar, P., Collett, T. S., Boswell, R., Cochran, J. R., Lall, M., Mazumdar, A., Ramana, M.V., Ramprasad, T., Riedal, M., Sain, K., Sathe, A., V., Vishwanath, K., Yadav, U.S., NGHP Expedition 01 Scientific Party., 2014. Geologic implications of gas hydrates in the offshore of India: Krishna–Godavari basin, Mahanadi basin, Andaman Sea, Kerala–Konkan basin. *Marine and Petroleum Geology*, 58, 29-98.
27. Lisé-Pronovost, A., St-Onge, G., Brachfeld, S., Barletta, F., Darby, D., 2009. Paleomagnetic constraints on the Holocene stratigraphy of the Arctic Alaskan margin. *Global and Planetary Change* 68, 85–99.
28. Liu, Q., Roberts, A. P., Torrent, J., Horng, C-S., Larrasoña, J. C., 2007. What do the HIRM and S-ratio really measure in environmental magnetism? *Geochemistry Geophysics Geosystems*, 8, Q09011.
29. Lund, S. P., Banerjee, S. K., 1985. Late Quaternary paleomagnetic field secular variation from two Minnesota lakes. *Journal of Geophysical Research: Solid Earth* 90(B1), 803-825.

30. Maher, B. A., 1988. Magnetic properties of some synthetic sub-micron magnetites. *Geophysical Journal International* 94, 83–96.
31. Mazumdar, A., Dewangan, P., João, H.M., Peketi, A., Khosla, V.R., Kocherla, M., Badesab, F.K., Joshi, R.K., Roxanne, P., Ramamurty, P.B., Karisiddaiah, S.M., Patil, D.J., Dayal, A.M., Ramprasad, T., Hawkesworth, C.J., Avanzinelli, R., 2009. Evidence of paleo-cold seep activity from the Bay of Bengal, offshore India. *Geochemistry Geophysics Geosystems* 10, Q06005.
32. Mazumdar, A., João, H.M., Peketi, A., Dewangan, P., Kocherla, M., Joshi, R.K., Ramprasad, T., 2012. Geochemical and geological constraints on the composition of marine sediment pore fluid: possible link to gas hydrate deposits. *Marine and Petroleum Geology* 38, 35–52.
33. McFadden, P.L., Merrill, R.T., 1995. History of Earth's magnetic field and possible connections to core-mantle boundary processes. *Journal of Geophysical Research* 100, 307–316.
34. Merrill, R.T., McElhinny, M.W., McFadden, P.L., 1996. *The Magnetic Field of the Earth*, 531 pp., Academic, San Diego, California.
35. NIO, 2005. Geoscientific investigations of shallow sediments in KG offshore, east coast. Tech. Rep no NIO/TR-13/2003. National Institute of Oceanography, Dona-Paula, Goa.
36. Nourgaliev, D. K., Heller, F., Borisov, A. S., Hajdas, I., Bonani, G., Iassonov, P. G., Oberhänsli, H., 2003. Very high resolution paleosecular variation record for the last~ 1200 years from the Aral Sea. *Geophysical Research Letters*, 30(17), 1914.
37. Nurgaliev, D.K., Borisov, A.S., Heller, F., Burov, B.V., Jasonov, P.G., Khasanov, D.I., Ibragimov, S.Z., 1996. Geomagnetic secular variation through the last 3500 years as recorded by lake Aslikul sediments from eastern Europe (Russia). *Geophysical Research Letters* 23, 375–378.
38. Ojha, P.S., Dubey, M., 2006. Giant hydrocarbon fields of offshore Krishna-Godavari basin. Petroview, an inhouse Journal Director General of Hydrocarbons 1, 26–30.
39. Oldfield, F., Yu, L., 1994. The influence of particle size variations on the magnetic properties of sediments from the north-eastern Irish Sea. *Sedimentology* 41, 1093 - 1108.
40. Opdyke, N. D., 1972. Paleomagnetism of deep-sea cores. *Review of Geophysics and Space Physics*, 10, 213-249.
41. Peck, J.A., King, J.W., Colman, S., M., Kravchinsky, V., A., 1996. An 84-kyr paleomagnetic record from the sediments of Lake Baikal, Siberia. *Journal of Geophysical Research* 101 (B5), 11365–11385.
42. Peketi, A., Mazumdar, A., Joao, H., M., Patil, D., J., Usapkar, A., Dewangan, P., 2015. Coupled C-S-Fe geochemistry in a rapidly accumulating marine sedimentary system: Diagenetic and depositional implications. *Geochemistry, Geophysics, Geosystems*. Doi: 10.1002/2015GC005754.
43. Powell, C.M., Roots, S.R., Veevers, J.J., 1988. Pre-breakup continental extension in east Gondwanaland and the early opening of the eastern Indian Ocean. *Tectonophysics* 155, 261–283.
44. Prabhakar, K.N., Zutshi, P.L., 1993. Evolution of southern part of Indian east coast basins. *Journal of Geological Society of India* 41, 215–230.
45. Ramana M.V., Nair R.R., Sarma K.V.L.N.S., Ramprasad T., Krishna K.S., Subrahmanyam V., D'Cruz M., Subrahmanyam C., Paul J., Subrahmanyam A. S., Sekhar, D.V.C., 1994. Mesozoic anomalies in the Bay of Bengal. *Earth and Planetary Science Letters* 121, 469–475.

46. Ramana, M.V., Ramprasad, T., Paropkari, A.L., Borole, D. V, Rao, B.R., Karisiddaiah, S.M., Desa, M., Kocherla, M., Joao, H.M., Lokabharati, P., Gonsalves, M.J., Pattan, J.N., Khadge, N.H., Prakash Babu, C., Sathe, A. V, Kumar, P., Sethi, A.K., 2009. Multidisciplinary investigations exploring indicators of gas hydrate occurrence in the Krishna–Godavari basin offshore, east coast of India. *Geo-Marine Letters*. 29, 25–38.
47. Ramprasad, T., Dewangan, P., Ramana, M.V., Mazumdar, A., Karisiddaiah, S.M., Ramya, E.R., Sriram, G., 2011. Evidence of slumping/sliding in Krishna–Godavari offshore basin due to gas/fluid movements. *Marine and Petroleum Geology* 28, 1806–1816.
48. Rao, G.N., 2001. Sedimentation, stratigraphy, and petroleum potential of Krishna-Godavari basin, east coast of India. *American Association of Petroleum Geology Bulletin* 85, 1623–1643.
49. Rao, V.P., 1991. Clay mineral distribution in the continental shelf and slope off Saurashtra, west coast of India. *Indian Journal of Marine Sciences* 20, 1–6.
50. Roberts, A. P., Reynolds, R. L., Verosub, K. L., & Adam, D. P., 1996. Environmental magnetic implications of greigite (Fe₃S₄) formation in a 3 my lake sediment record from Butte Valley, northern California. *Geophysical Research Letters*, 23(20), 2859-2862.
51. Roberts, A.P., Tauxe, L., Heslop, D., 2013. Magnetic paleointensity stratigraphy and high-resolution Quaternary geochronology: successes and future challenges. *Quaternary Science Reviews* 61, 1–16.
52. Sagnotti, L., Smedile, A., De Martini, P.M., Pantosti, D., Speranza, F., Winkler, A., Carlo, P. Del., Bellucci, L.G., Gasperini, L., 2011. A continuous palaeosecular variation record of the last four millennia from the Augusta Bay (Sicily, Italy). *Geophysical Journal International* 184, 191–202.
53. Sangode, S.J., Sinha, R., Phartiyal, B., Chauhan, O.S., Mazari, R.K., Bagati, T.N., Suresh, N., Mishra, S., Kumar, R., Bhattacharjee, P., 2007. Environmental magnetic studies on some quaternary sediments of varied depositional settings in the Indian sub-continent. *Quaternary International* 159, 102–118.
54. Sastri, V.V., Venkatachala, B. S., Narayanan, V., 1981. The evolution of the east coast of India. *Palaeogeography, Palaeoclimatology, Palaeoecology*, 36(1), 23-54.
55. Scotese, C.R., Gahagan, L.M., Larson, R.L., 1988. Plate tectonic reconstructions of the Cretaceous and Cenozoic ocean basins. *Tectonophysics* 155, 27–48.
56. Snowball, I. F., 1997. Gyromagnetic magnetization and the magnetic properties of greigite-bearing clays in southern Sweden. *Geophysical Journal International*, 129(3), 624-636.
57. Snowball, I., Sandgren, P., 2002. Geomagnetic field variations in northern Sweden during the Holocene quantified from varved lake sediments and their implications for cosmogenic nuclide production rates. *The Holocene* 12, 517-530.
58. Snowball, I., Zillén, L., Ojala, A., Saarinen, T., Sandgren, P., 2007. FENNOSTACK and FENNORPIS: varve dated Holocene palaeomagnetic secular variation and relative palaeointensity stacks for Fennoscandia. *Earth and Planetary Science Letters* 255, 106–116.
59. Sprowl, D. R., Banerjee, S. K., 1989. The Holocene paleosecular variation record from Elk Lake, Minnesota. *Journal of Geophysical Research: Solid Earth* 94(B7), 9369-9388.
60. Stockhausen, H., 1998. Geomagnetic palaeosecular variation (0 -13 000 yr BP) as recorded in sediments from three maar lakes from the West Eifel (Germany) 135, 898–910.

61. St-Onge, G., Stoner, J.S., Hillaire-Marcel, C., 2003. Holocene paleomagnetic records from the St. Lawrence Estuary, eastern Canada: centennial- to millennial-scale geomagnetic modulation of cosmogenic isotopes. *Earth and Planetary Science Letters* 209, 113–130.
62. Thompson, R., Oldfield, F., 1986. *Environmental Magnetism*. Allen and Unwin, London.
63. Thompson, R., 1975. Long period European geomagnetic secular variation confirmed. *Geophysical Journal International*, 43(3), 847-859.
64. Turner, G.M., Thompson, R., 1981. Lake sediment record of the geomagnetic secular variation in Britain during Holocene times. *Geophysical Journal International*, 65(3), 703-725.
65. Turner, G. M., Thompson, R., 1982. Detransformation of the British geomagnetic secular variation record for Holocene times. *Geophysical Journal of the Royal Astronomical Society*, 70(3), 789-792.
66. Usapkar, A., Dewangan, P., Kocherla, M., Ramprasad, T., Mazumdar, A., Ramana, M.V., 2014. Enhanced methane flux event and sediment dispersal pattern in the Krishna–Godavari offshore basin: evidences from rock magnetic techniques. *Marine and Petroleum Geology* 58, 461–475.
67. Verosub, K. L., Mehringer, JR. P. J., Waterstraat, P., 1986. Holocene secular variation in Western North America: paleomagnetic record from Fish lake, Harney County, Oregon. *Journal of Geophysical Research: Solid Earth* 91(B3), 3609-3623.
68. Vigliotti, L., 2006. Secular variation record of the Earth’s magnetic field in Italy during the Holocene: constraints for the construction of a master curve. *Geophysics Journal International* 165, 414–429.
69. Walden, J., Oldfield, F., Smith, J.P. (eds.), 1999. *Environmental magnetism: a practical guide*. Technical Guide, N0. 6. Quaternary Research Association, London.
70. Yang, X., Heller, F., Yang, J., Su, Z., 2009. Paleosecular variations since ~9000 yr BP as recorded by sediments from maar lake Shuangchiling, Hainan, South China. *Earth and Planetary Science Letters* 288, 1–9.
71. Yang, X., Yang, J., Su, Z., Huang, W., Wang, J., 2013. Paleosecular variations refining the chronology of the sediments from the Pearl River Delta, southern China. *The Holocene* 23, 635–644.
72. Zheng, Y., Zheng, H., Deng, C., Liu, Q., 2014. Holocene paleomagnetic secular variation from East China sea and a PSV stack of East Asia. *Physics of the Earth and Planetary Interiors*, 236, 69-78.
73. Zijderveld, J.D.A., 1967. A.C. demagnetisation of rock: analysis of results, in *Methods in paleomagnetism*, edited by D.W., Collinson, K.M., Creer, S.K., Runcorn. Elsevier, Amsterdam, the Netherlands, pp. 254–286.

74. Figure captions

Fig. 1. Location map of the study area in the Krishna-Godavari offshore basin, Bay of Bengal. The black stars represent core locations MD161/8, MD161/11 and MD161/13. The zoom out of the study area is shown in the inset.

Fig. 2. Orthogonal Zijderveld vector end plots of representative samples of A) MD161/8 B) MD161/11 and C) MD161/13. Circles and squares represent projection on the vertical and horizontal plane, respectively.

Fig. 3. Paleoinclination, relative paleodeclination and paleointensity records of a) MD161/8 (MD8), b) MD161/11 (MD11) and c) MD161/13 (MD13) with respect to depth below the seafloor.

Fig. 4. The comparison of a) paleoinclination, b) relative paleodeclination and c) paleointensity records from MD161/8, MD161/11 and MD161/13 cores with respect to age in cal. kyr BP.

Fig. 5. Downcore variation of A) χ_{LF} , B) χ_{ARM} and C) SIRM of core MD161/13 with respect to age in cal. kyr. BP.

Fig. 6. Downcore variation of A) $\chi_{fd}\%$, B) ARM/SIRM, C) SIRM/ χ_{LF} , D) S-ratio, E) Softirm and F) Hirm of core MD161/13 with respect to age in cal. kyr. BP.

Fig. 7. Cross plots of SIRM and χ_{LF} of A) MD161/8 and B) MD161/13.

Fig. 8. Temporal variation of a) paleoinclination, b) relative paleodeclination records from MD161/8, MD161/11, MD161/13 (sediment cores from Bay of Bengal, India) and SCL lake (China, modified after Yang et al., 2009) and Biwa lake (Japan, modified after Ali et al., 1999). The CALS7k.2 and CALS10k.1b models show good correlation with Biwa lake record as it was considered during the modeling (Korte et al., 2011).

Fig. 9. Inclination anomaly computed from a) CALS7k.2 and b) CALS10k.1b model at 0.6, 2.2, 4.3 and 5.8 cal. kyr BP. The inclination anomaly represents the contribution from non-axial dipolar components of earth's magnetic field. The field appears to be strongest over the Bay of Bengal with limited spatial extent.

Table captions

Table 1. Paleoinclination, relative paleodeclination, paleointensity records of A) MD161/8, B) MD161/11 and C) MD161/13.

Table 2. Variations in rock magnetic parameters for MD161/13 core.

Table 3. Average values and standard deviation of different rock magnetic parameters for MD161/13 and MD161/8 cores.

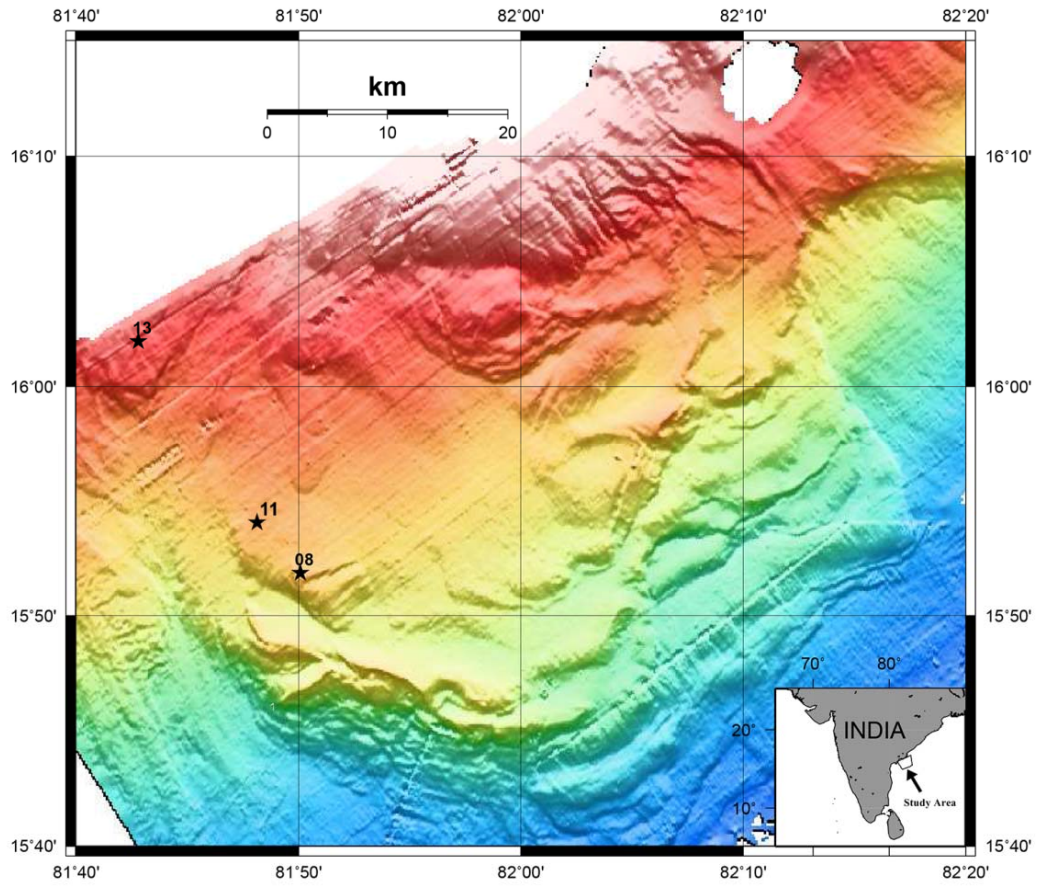


Figure 1

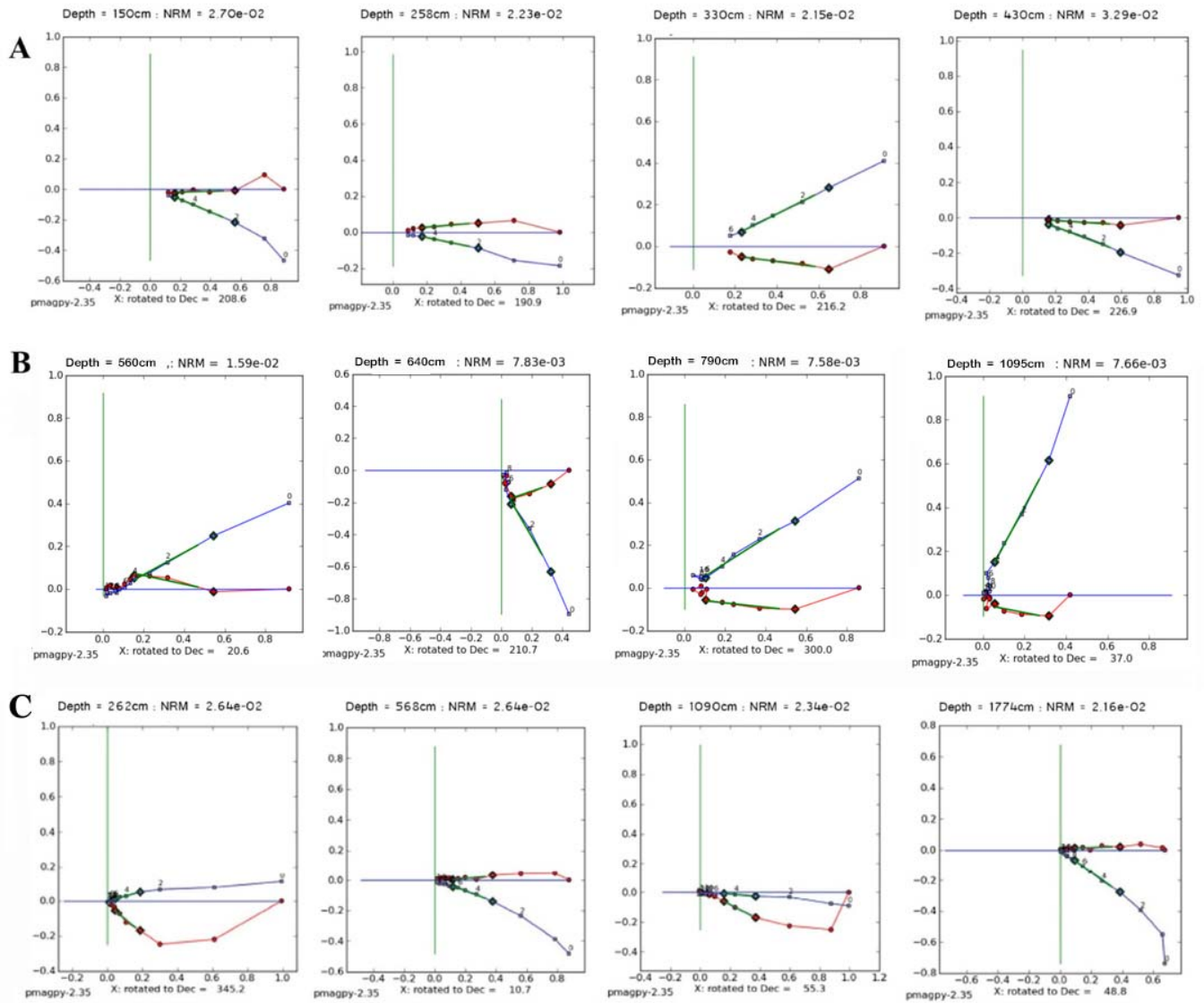


Figure 2

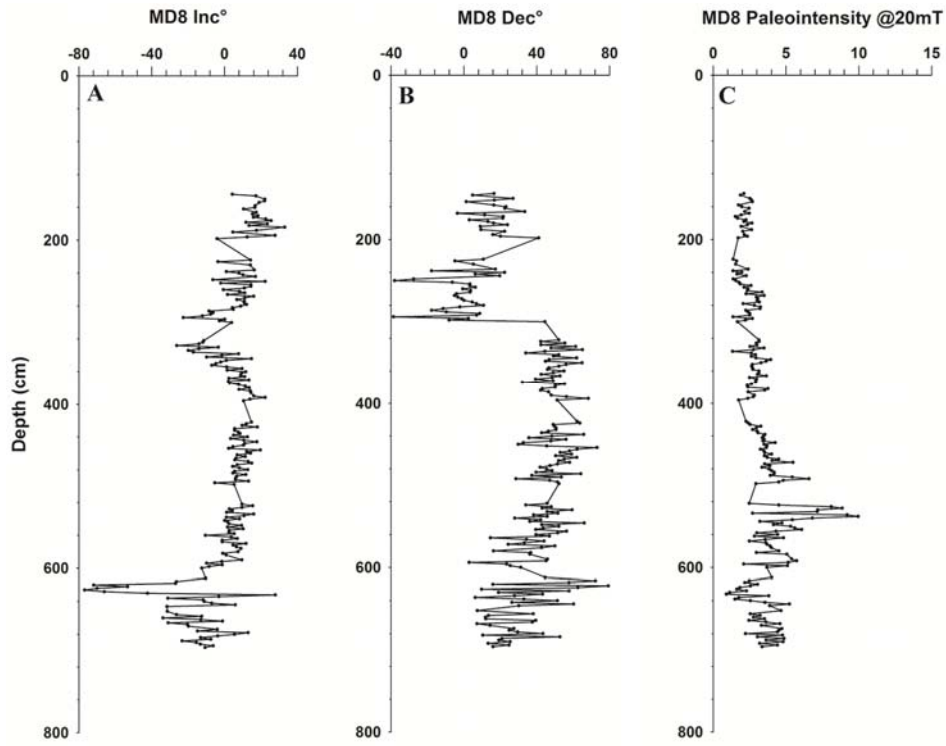


Figure 3A

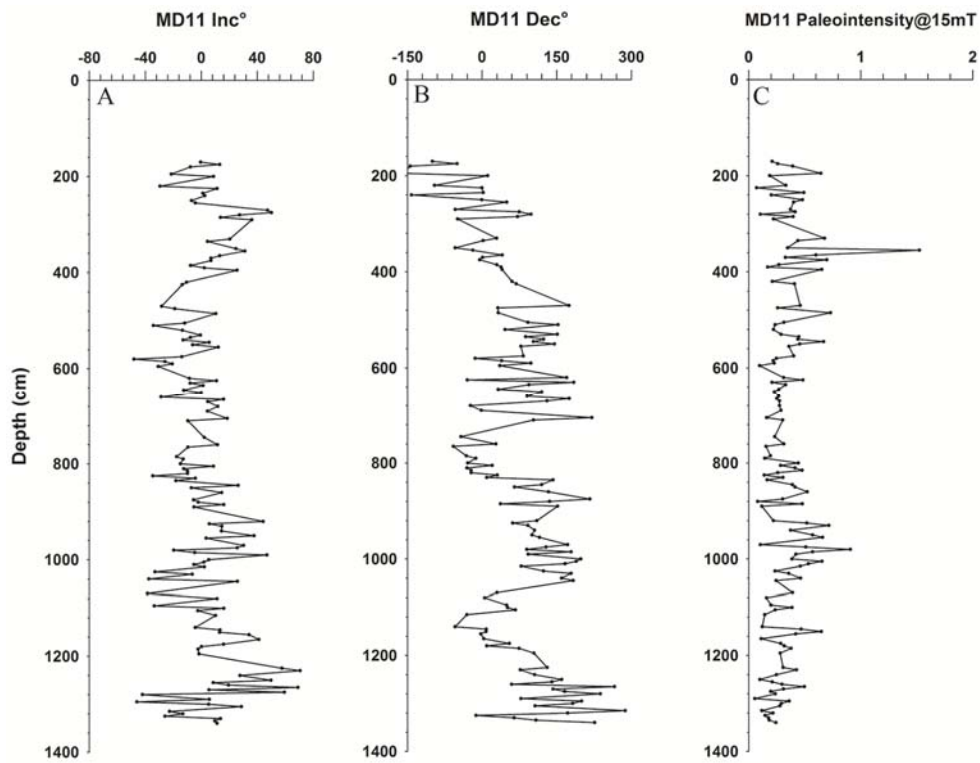


Figure 3B

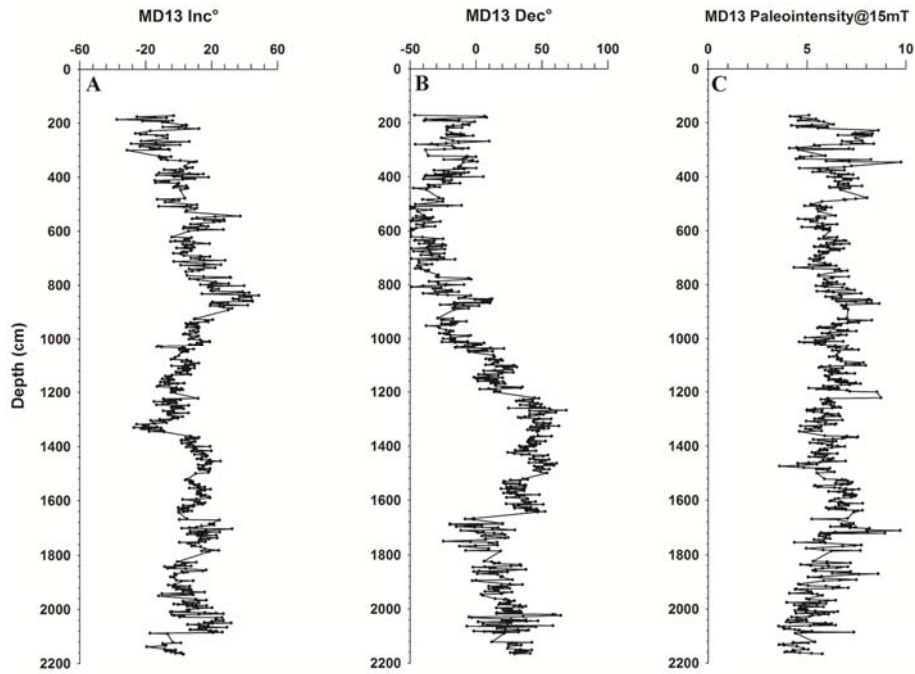


Figure 3C

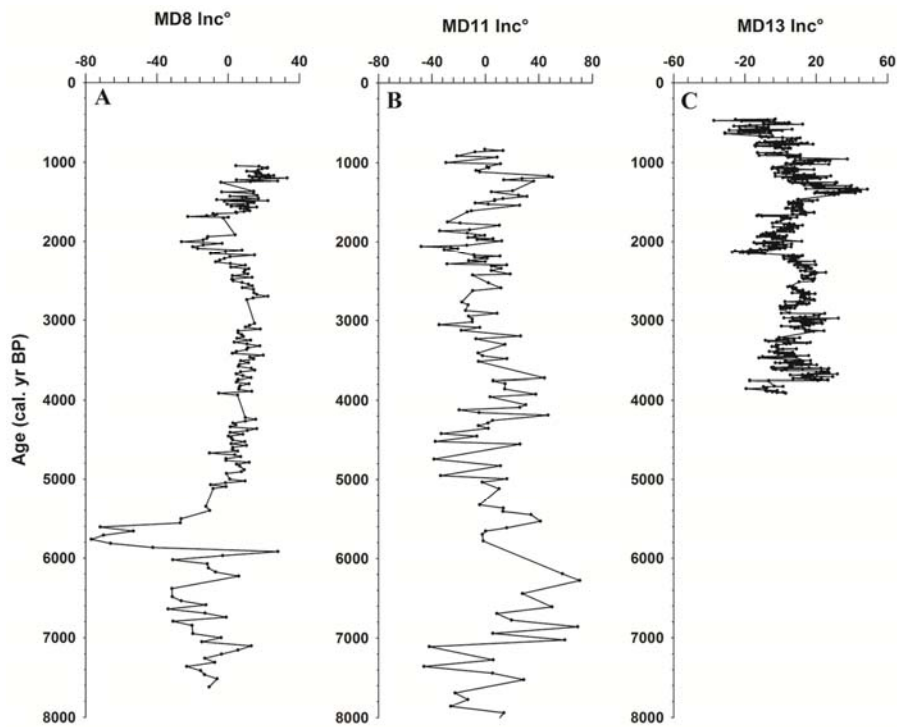


Figure 4A

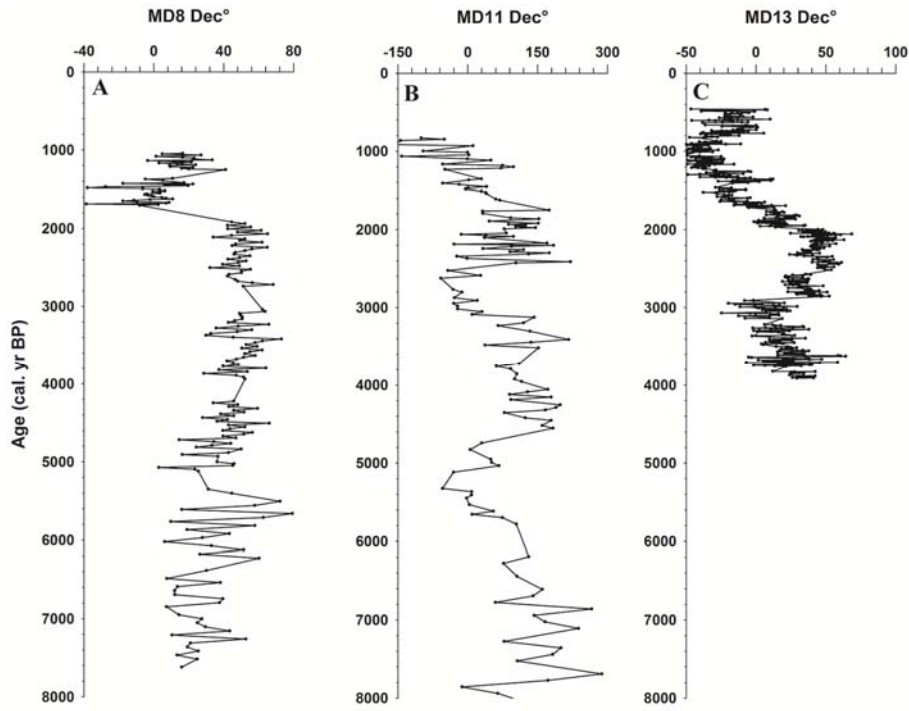


Figure 4B

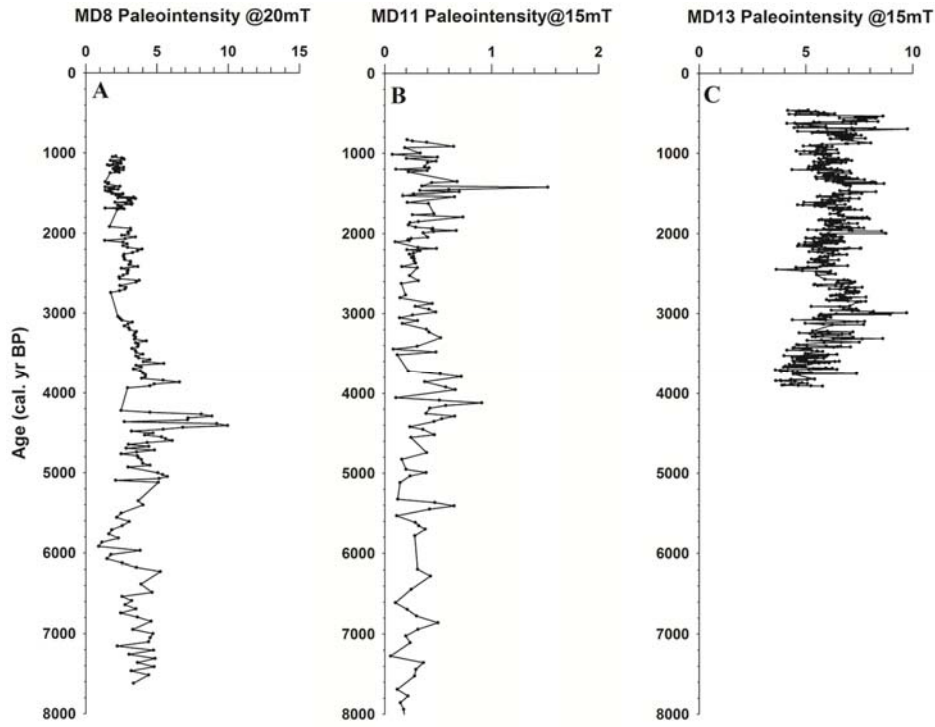


Figure 4C

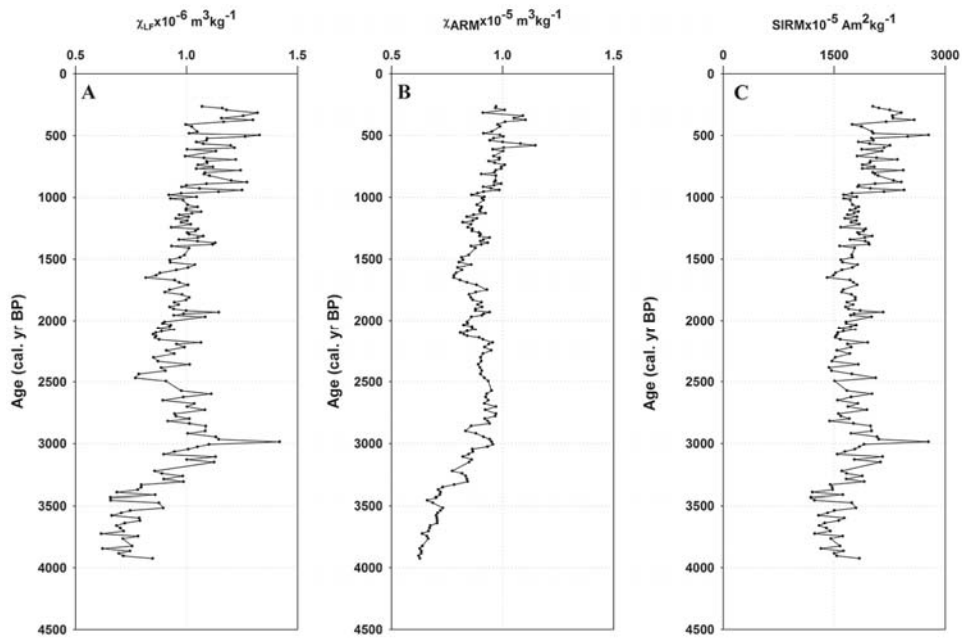


Figure 5

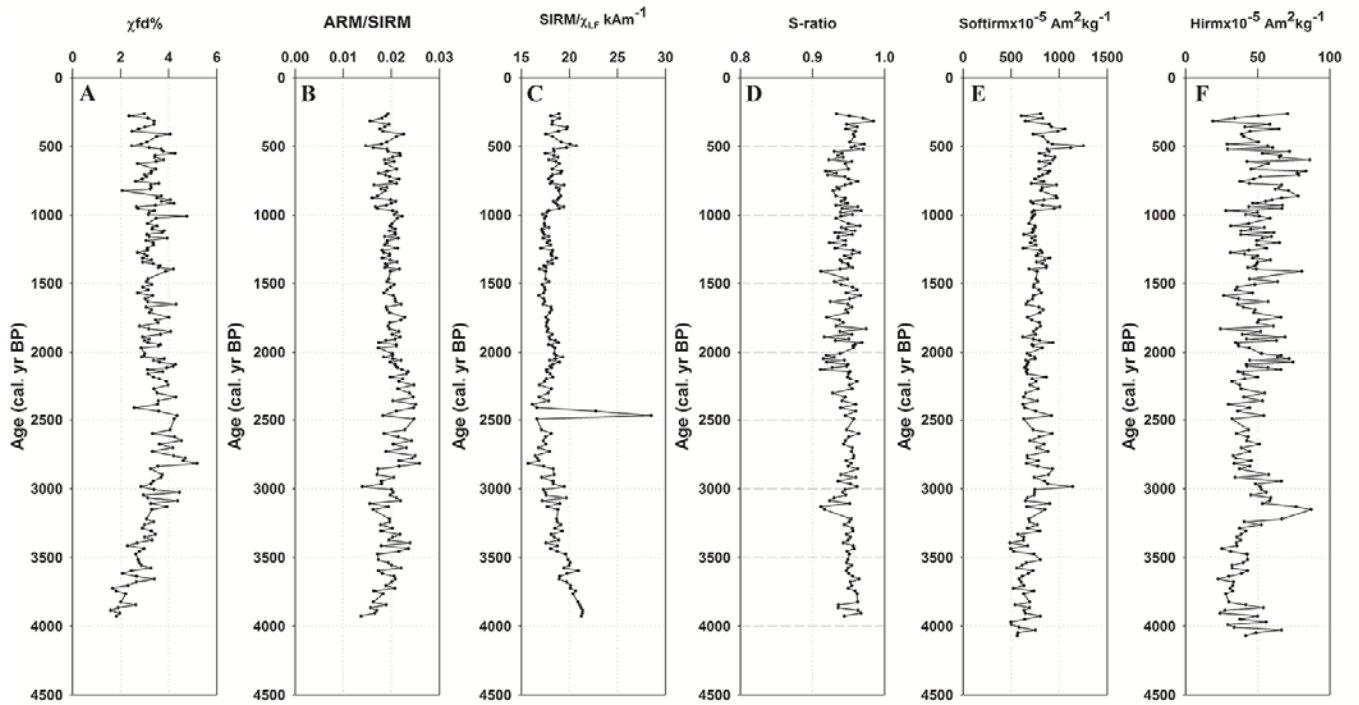


Figure 6

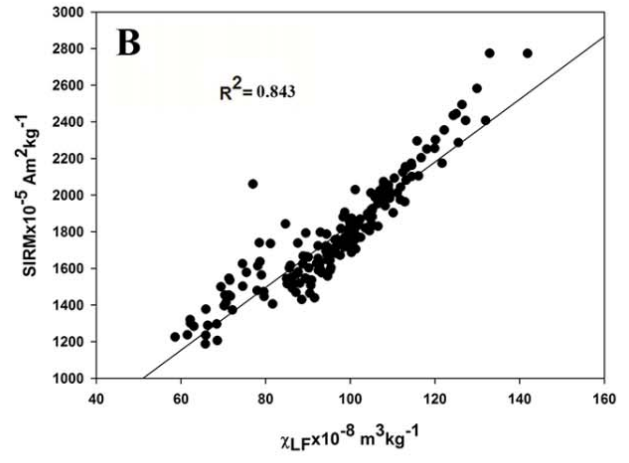
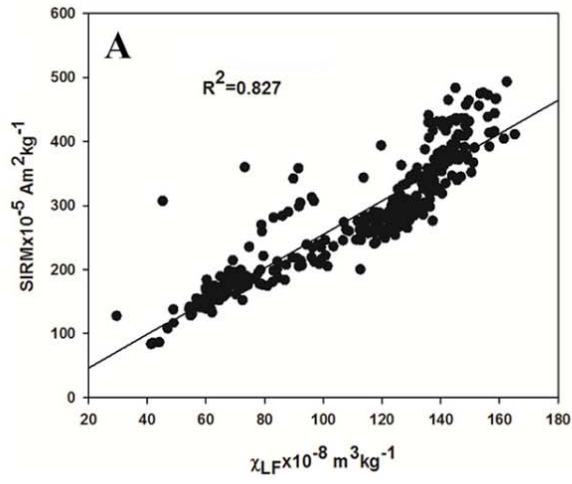


Figure 7

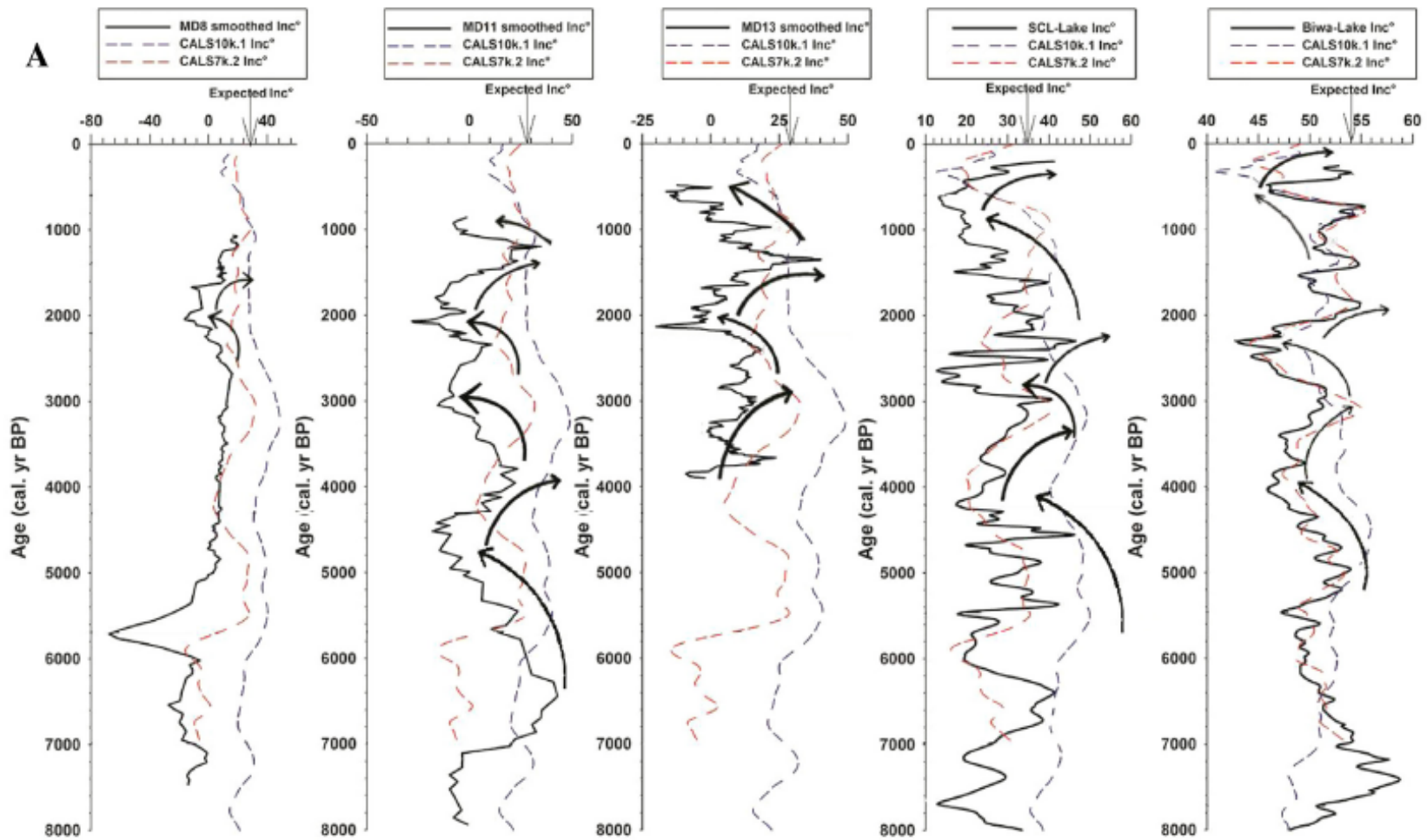


Figure 8A

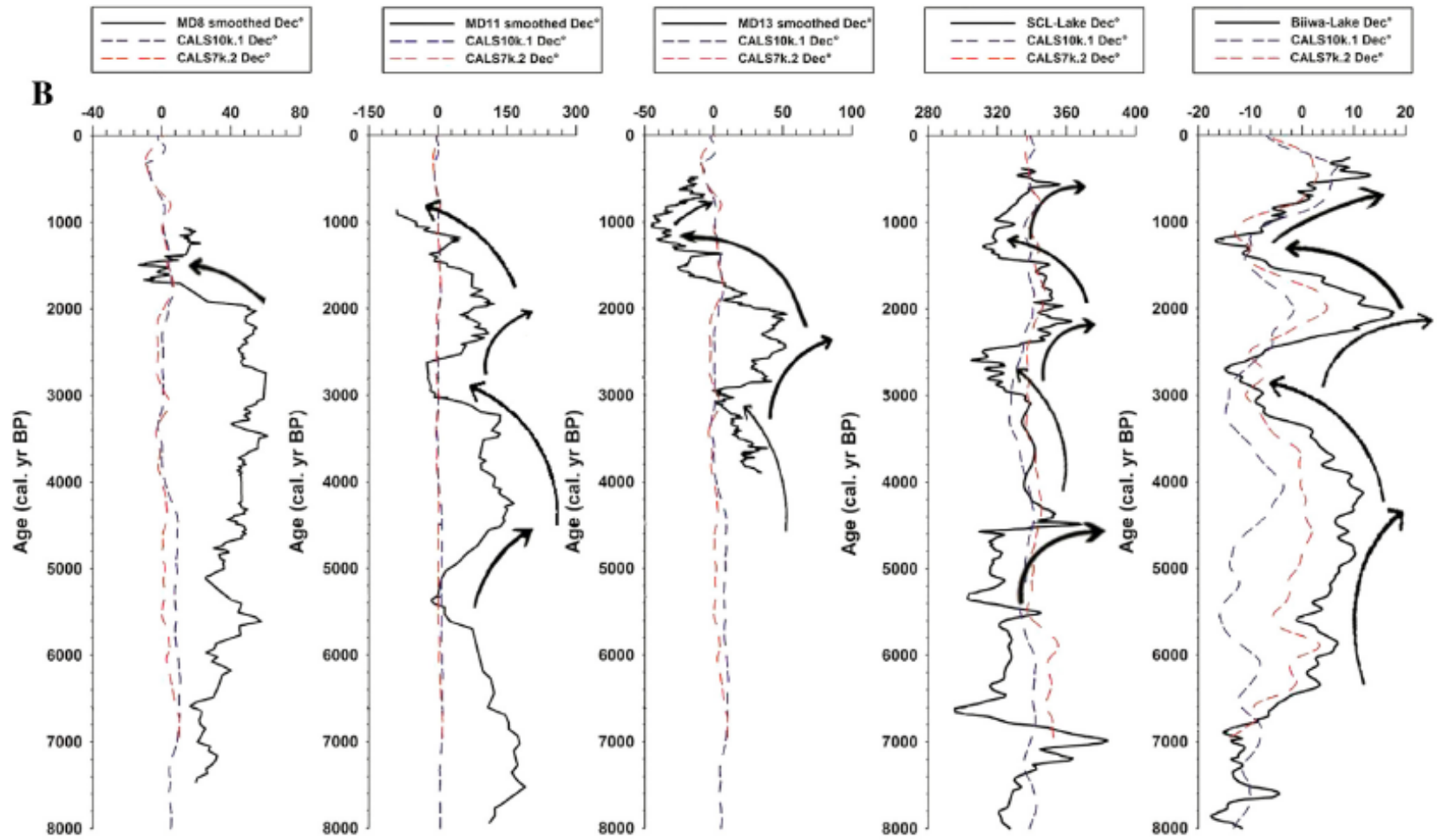


Figure 8B

A

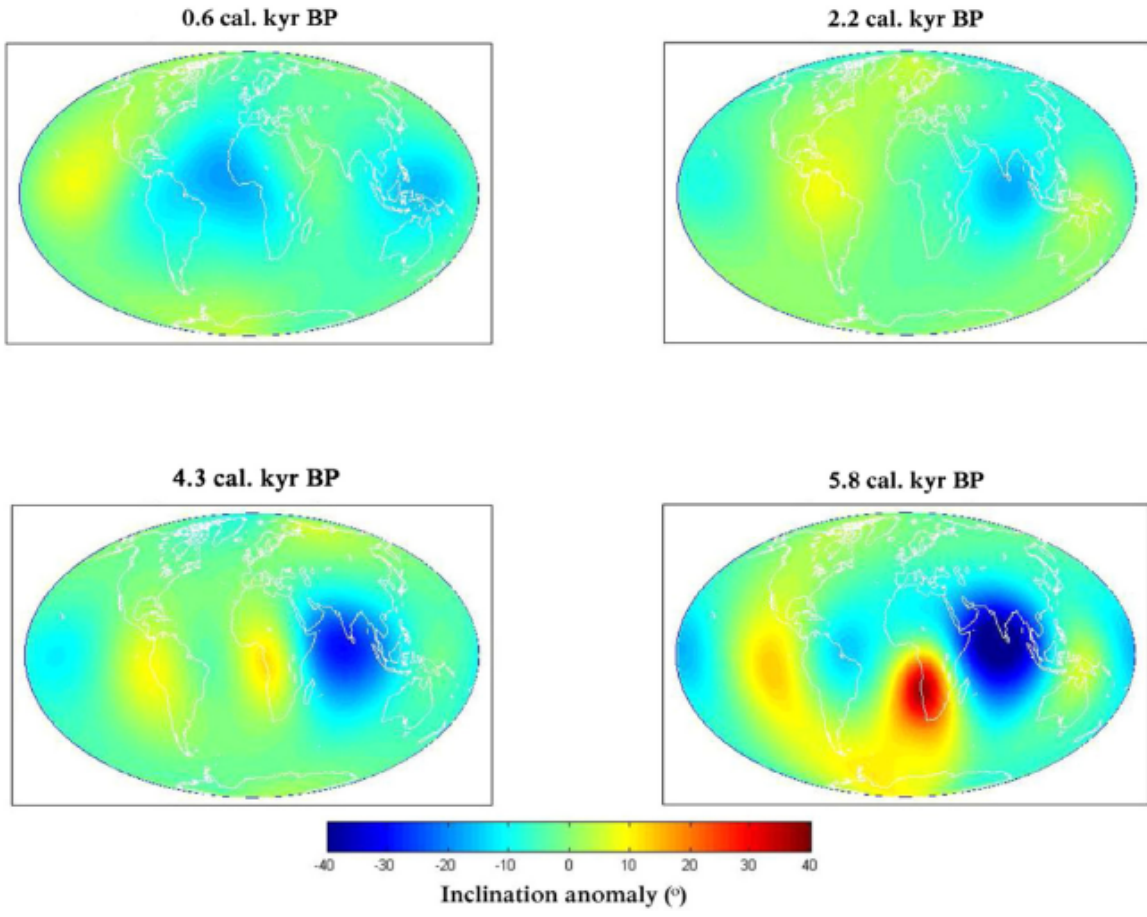


Figure 9A

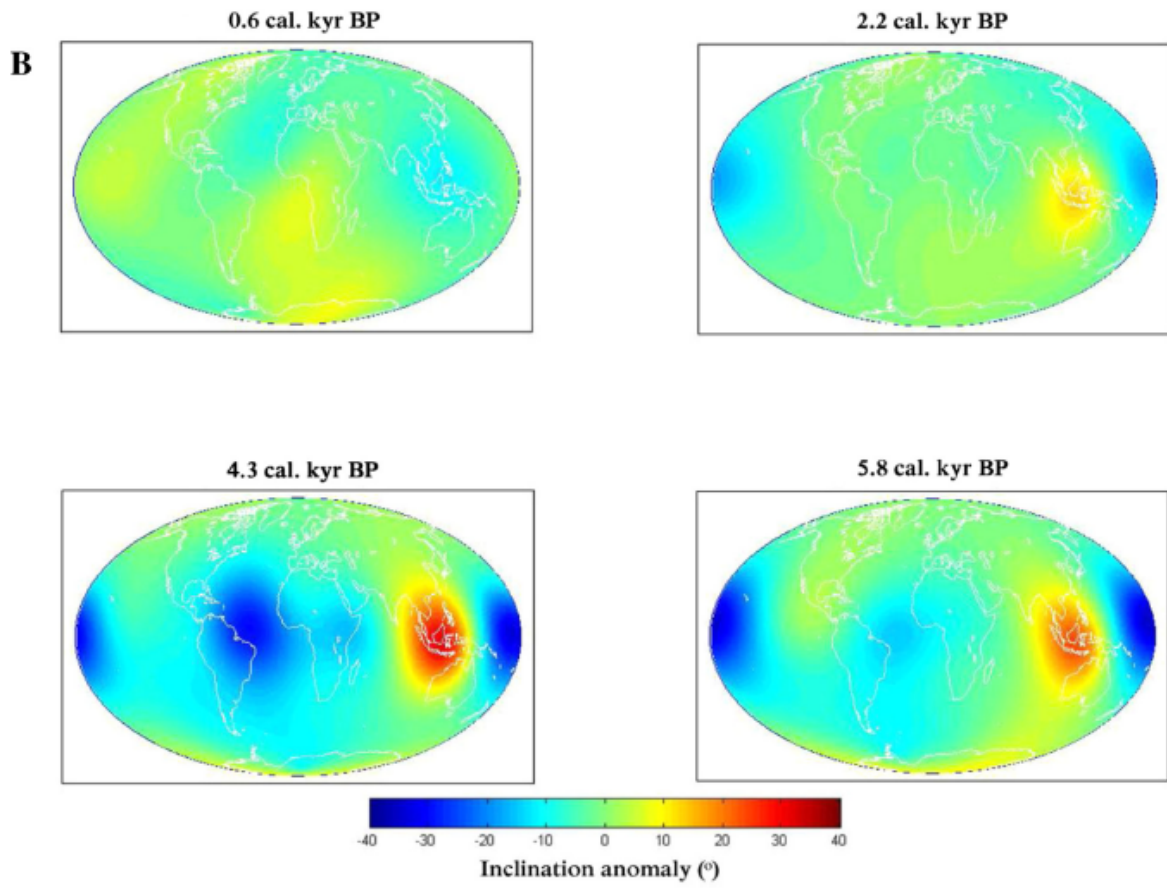


Figure 9B

Table 1: Paleoinclination, relative paleodeclination and paleointensity records of A) MD161/8, B) MD161/11, C) MD161/13

		MD161/8			
Depth in m	Interpolated age	Inc °	Relative	MAD	RPI
	in cal Yr BP		Dec°		20mT
1.44	1044.0	4.3	16.5	3	2.1111
1.46	1051.7	17.3	4.8	2	1.8801
1.5	1067.2	22.1	27	2.3	2.524
1.52	1075.0	22	16.7	1.5	2.6405
1.54	1082.7	19	1.3	3.5	2.6934
1.58	1098.2	16.8	16.4	1.7	1.7396
1.6	1105.9	16.7	23.1	2.4	1.9599
1.62	1113.7	10.5	22.5	1.8	2.4613
1.66	1129.1	17.4	33.4	4.1	2.1677
1.68	1136.9	15.4	-3.5	5.2	2.4765
1.7	1144.6	18.4	11.4	4	1.9212
1.72	1152.4	15.9	21.6	2.9	1.5312
1.74	1160.1	22.6	21.4	4.3	1.6789
1.76	1167.8	25.6	3	5.5	2.2618
1.78	1175.6	11.8	13.2	7.3	2.1065
1.8	1183.3	23.5	16.3	7.4	2.6614
1.82	1191.1	13.5	23.9	6.2	2.3495
1.84	1198.8	33.1	9	5.6	1.9198
1.88	1214.3	17.6	9.4	3.5	2.6367
1.9	1222.0	4.6	22.4	3.1	2.039
1.94	1237.5	27.8	15.9	2.7	2.1399
1.96	1245.2	12.5	20.1	4.8	2.3501
1.98	1253.0	-4.1	41.1	0.9	1.7199
2.24	1366.4	14.3	10.7	3.9	1.3788
2.26	1375.5	-3.6	-4.9	0.7	1.6041
2.3	1393.7	14.2	5.2	1.4	1.5496
2.36	1421.1	16.3	17.3	1.2	2.4023
2.38	1430.2	1	-17.7	1.5	1.3649
2.4	1439.3	8	22.4	1.8	1.9724
2.42	1448.4	10.1	6.2	1.1	1.6307
2.44	1457.6	17	19.7	3.9	2.2749
2.48	1473.0	-6.4	-27.6	5.6	1.3827
2.5	1484.9	22.3	-38	1.4	1.5652
2.52	1494.0	-2.1	-6.3	2.2	1.7734
2.54	1503.2	14.5	3.3	1.8	1.8628
2.56	1512.3	14.5	3.3	1.8	2.604
2.58	1521.4	10.9	6.3	1.2	2.1238
2.6	1530.5	-0.6	-0.6	1	2.3951

2.62	1539.6	8.2	3.7	2.5	2.3396
2.64	1548.8	11.1	3.4	2.6	3.3649
2.66	1557.9	1.7	-4	2.7	2.2672
2.68	1567.0	16	-5.2	2.9	3.4985
2.7	1576.1	11.1	-3.3	3.7	2.9733
2.72	1585.2	6.8	-1.2	4.5	3.061
2.74	1594.4	10.9	0.1	5.7	3.0216
2.76	1603.5	10.8	4.6	6.3	3.1714
2.78	1612.6	12.1	6.9	1.5	2.06
2.8	1621.7	8.9	10.8	2.4	2.8332
2.82	1630.8	4.3	-2.1	5	3.2524
2.84	1640.0	4.8	-11.4	3.5	3.218
2.86	1649.1	-8.5	-17.7	5.7	2.2453
2.88	1658.2	-6.3	-9.6	0.9	2.3949
2.9	1667.3	-7.6	8.7	3.2	2.5169
2.92	1676.4	-12.1	7	5.9	2.5112
2.94	1685.6	-22.6	-38.7	4.8	1.364
2.96	1694.7	0.1	2.5	2.4	2.6929
2.98	1703.8	-2.8	-8.1	3.5	2.2095
3	1917.2	3.9	44.5	2.6	1.6715
3.22	1938.9	-11.4	52.1	3	3.1412
3.24	1960.6	-11.9	42.2	3.1	3.1547
3.26	1982.4	-14	55.4	4	2.9708
3.28	2004.1	-26.2	42.3	1.6	3.0059
3.3	2025.8	-3.4	61.4	7.4	2.534
3.32	2047.5	-14	47.9	3.8	3.4935
3.34	2069.2	-19.9	65.1	5.1	2.7593
3.36	2091.0	-17.1	44.5	3	1.3391
3.38	2112.7	7.7	34	5.1	2.6279
3.4	2134.4	-1.4	52.1	3.7	2.9084
3.42	2156.1	-9.8	49.2	3	2.6184
3.44	2177.8	14.8	61.9	1.8	2.9444
3.46	2199.6	1	46.9	2.4	3.9473
3.48	2221.3	-2.1	44.8	2.9	3.6364
3.5	2243.0	-4.7	64.9	3.1	3.2835
3.52	2264.7	-7	56.1	1.4	2.6955
3.54	2286.4	1.2	52.2	1.9	2.6461
3.56	2308.2	9.6	46.7	1.2	2.7037
3.58	2329.9	1.5	45.9	2.2	2.7329
3.6	2351.6	11.6	55	1.4	3.1396
3.62	2373.3	9.3	49.1	3.3	3.1456
3.64	2395.0	8.8	42.4	3.2	3.0471
3.66	2416.8	11.1	52.8	2.6	3.6499
3.68	2438.5	2.4	48.4	2.6	2.5006

3.7	2460.2	13.4	39.4	2.5	2.9795
3.72	2481.9	2.1	49	2.5	2.9326
3.74	2503.6	2.8	32.1	3	2.9218
3.76	2525.4	7.8	55.3	5.9	2.6355
3.78	2547.1	11.4	50.2	1.5	2.342
3.8	2568.8	13.6	50.1	0.8	2.3882
3.82	2590.5	8	43.1	2.3	3.7622
3.84	2612.2	14.2	42.1	1.3	3.5405
3.86	2655.7	14.5	46.5	1.4	2.4008
3.9	2677.4	16.1	48	2.7	2.8249
3.92	2699.1	22.3	56.3	1.8	2.7598
3.94	2720.8	14	68.3	2.5	2.3798
3.96	2742.6	10.5	51.2	4.3	1.7524
4.22	3042.3	14.8	62.2	2.9	2.2624
4.24	3065.9	12	63.7	3.8	2.4054
4.26	3089.5	9.7	49.1	3.3	2.5418
4.28	3113.1	18	49.7	1.7	3.2691
4.3	3136.7	5.6	50.6	5.7	2.9685
4.32	3160.3	5.6	50.6	5.7	2.7054
4.34	3183.9	7.5	46.4	1.6	3.0197
4.36	3207.5	8.5	42.7	2.9	3.0849
4.38	3231.1	5	65.8	2.2	3.5549
4.4	3254.7	12.6	48.3	2.1	3.4661
4.42	3278.3	3.4	35.7	1.8	3.3797
4.44	3301.9	10.6	56.1	6.2	3.504
4.46	3325.5	17.8	47.8	2.4	3.4223
4.48	3349.1	11.1	32.7	3.8	4.2551
4.5	3372.7	10.4	29.8	1.7	3.4984
4.52	3396.3	4.6	45.5	2.5	3.6905
4.54	3419.9	2.3	73.1	3.5	3.6537
4.56	3443.5	19.7	62.2	3.7	3.2462
4.58	3467.1	12.2	58	1.7	3.4816
4.6	3490.7	14.3	52.9	3.7	3.5404
4.62	3514.3	7	59.1	4	4.0122
4.64	3537.9	11.4	50.4	4.5	3.5249
4.66	3561.5	6.3	62	4.3	3.7123
4.68	3585.1	5.7	55.1	2	4.499
4.7	3608.7	13	52	3.6	4.0476
4.72	3632.3	14.9	58	2.4	5.4815
4.74	3655.9	7	51.4	2.9	3.54
4.76	3679.5	4.5	47.3	2.1	3.8947
4.78	3703.1	8.2	41.9	2.5	3.3581
4.8	3726.7	12.8	45.4	2.5	3.8322
4.82	3750.3	5.6	48.4	4.3	4.0057

4.84	3773.9	4.6	39.6	1.6	4.189
4.86	3797.5	11.7	64.2	3.3	4.1869
4.88	3821.1	6.7	37.3	1.3	3.9283
4.9	3844.7	6.2	53.5	0.8	5.4275
4.92	3868.3	6	28.6	4.2	6.5805
4.94	3891.9	13.2	47.1	3.9	4.8127
4.96	3915.5	-5.3	51.4	1.7	4.5039
4.98	3939.1	5.3	52.2	2.6	2.9335
5.22	4222.3	9.6	45.8	3.1	2.4802
5.24	4245.9	15.5	34	4.3	4.5091
5.26	4269.5	9.6	48	5.8	8.0989
5.28	4293.1	2.7	43	2.8	8.8594
5.3	4316.7	4.3	59.4	5.6	7.1835
5.32	4340.3	1.2	45.7	1.5	7.1471
5.34	4363.9	16	51.6	3	2.7082
5.36	4387.5	10.7	38.3	1.6	9.2021
5.38	4411.1	1.1	45.8	2.5	9.9558
5.4	4434.7	8.3	27.9	1.9	6.8116
5.42	4458.3	0.1	42.1	4	5.4325
5.44	4481.9	1.8	36.2	1.5	3.2122
5.46	4505.5	2.5	66.1	2.8	4.7241
5.48	4529.1	9.4	42.8	2.3	4.1434
5.5	4552.7	1.7	52.1	1.8	5.3189
5.52	4576.3	10.2	43.6	1.5	5.6057
5.54	4599.9	2.6	39.5	2.4	6.0749
5.56	4623.5	2.4	56.4	0.9	4.3179
5.58	4647.1	5.3	51.5	3.3	2.9955
5.6	4670.7	-10.5	39.6	4.1	4.4286
5.62	4694.3	3.7	47	0.7	2.8397
5.64	4717.9	7	14.6	9.4	4.8248
5.66	4741.5	-1.2	34.3	3.9	3.5801
5.68	4765.1	-1.2	44	7	2.4896
5.7	4788.7	11.8	33.2	4.2	3.6234
5.72	4812.3	4.7	24.3	3.1	3.6991
5.74	4835.9	6.5	50	1.6	3.9034
5.76	4883.1	9	42.7	1.5	4.0026
5.8	4906.7	7.4	16.3	2	4.5133
5.82	4930.3	-1	36.7	5	2.9737
5.84	5001.1	0.9	36.2	1.2	5.0653
5.9	5024.7	9.5	45.9	1.9	5.3963
5.92	5048.3	-1.5	45.2	2.1	5.7323
5.94	5071.9	-9.8	2.9	3.4	5.1558
5.96	5095.5	-1.2	23.5	3.8	2.0993
5.98	5119.1	-8.4	25.5	1	5.0994

6	5351.6	-12.5	31.2	2.2	3.6931
6.12	5403.1	-10.4	44.6	2.1	4.0154
6.16	5506.3	-26.4	72.2	4.6	2.4847
6.18	5557.8	-26.9	57.7	4.4	2.1775
6.2	5609.4	-71.8	16	2.2	3.0507
6.22	5660.9	-53.2	79.3	1.5	2.5618
6.24	5712.5	-70	62.6	14.4	1.83
6.26	5764.1	-76.8	9.7	2.2	1.6277
6.28	5815.6	-66	57.8	2.9	2.2873
6.3	5867.2	-42.3	19	2.5	1.142
6.32	5918.7	27.9	43.2	2.7	0.9074
6.34	5970.3	-3.1	27.8	4.8	3.8192
6.36	6021.9	-31.1	6.2	1.5	1.7655
6.38	6073.4	-11.7	32.9	3.2	1.5003
6.4	6125.0	-11.1	51.4	3.1	2.5569
6.42	6176.5	-7.1	26.4	3.4	3.5634
6.44	6228.1	5.9	60.2	2.8	5.2412
6.46	6382.8	-31.6	30.2	2.8	3.8778
6.52	6485.9	-31.4	7.4	3.1	4.6612
6.56	6537.5	-26.4	38.1	0.7	2.5474
6.58	6589.0	-12.5	13.5	2.8	3.2255
6.6	6640.6	-33.8	11.9	3.2	2.7719
6.62	6692.1	-13	12	2	3.5205
6.64	6743.7	-1.1	39.5	1.4	2.4598
6.66	6795.3	-31	37.6	5.1	3.6322
6.68	6846.8	-20.3	7.2	3.5	4.5873
6.7	6949.9	-19.8	14.4	0.4	3.3105
6.74	7001.5	-4	27.5	3.8	4.7228
6.76	7053.1	-14.8	24.9	4.9	4.5245
6.78	7104.6	13	29.5	4.5	4.4154
6.8	7156.2	5.5	43.4	1.9	2.2208
6.82	7207.7	-3.7	10.4	3.9	4.7632
6.84	7259.3	-13.1	52.7	4.5	3.0421
6.86	7310.9	-7.5	20.9	3.2	4.8645
6.88	7362.4	-23.3	19.2	2.9	3.6392
6.9	7414.0	-15.5	25.4	2.1	4.8021
6.92	7465.5	-13.3	13.3	3.8	3.1958
6.94	7517.1	-6.2	24.8	2.9	4.4164
6.96	7620.2	-10.7	16	2.7	3.3579

		MD161/11			
Depth in m	Interpolated age	Inc°	Relative	MAD	RPI
	in cal Yr BP		Dec°		15mT
1.7	830.4	-0.5	-99.8	6.4	0.2087
1.75	847.2	13.2	-50.3	6	0.2581
1.8	864.1	-7.7	-144.4	2.7	0.3927
1.95	914.5	-21.4	-159.6	4.1	0.644
2	931.3	8.8	11.3	2.9	0.1878
2.2	998.5	-29.5	-95.7	4.6	0.3312
2.25	1015.3	11.3	-0.1	12.5	0.0705
2.35	1049.0	1.1	2.4	5.2	0.4919
2.4	1065.8	2.5	-141.9	7.3	0.2013
2.5	1099.4	-7	-0.7	6.5	0.4804
2.55	1116.2	-4.2	49.6	3.5	0.4011
2.7	1166.6	47.4	-54	8.1	0.3722
2.75	1183.5	50.1	74.7	3.3	0.415
2.8	1200.3	27.4	98.2	3	0.1039
2.85	1217.1	13.7	71.3	8.8	0.3964
2.9	1233.9	36.1	-49.1	2.1	0.2205
3.3	1355.0	20.4	29.2	9	0.6768
3.35	1369.1	4.5	2.2	14.1	0.4398
3.5	1411.3	24.7	-53.9	16.1	0.3469
3.55	1425.4	31.1	-18.5	6.5	1.5251
3.65	1453.6	13.2	40.5	12.1	0.6001
3.7	1467.7	6.9	1	5.7	0.3279
3.75	1481.7	6.9	-4.8	4.9	0.6973
3.85	1509.9	-7.6	29.6	6.1	0.2695
3.9	1524.0	2.1	38.2	11.5	0.1694
3.95	1538.1	25.6	40.2	4.2	0.6521
4.2	1608.5	-10.5	60.1	7.7	0.2111
4.25	1622.6	-13.6	68.8	5.5	0.4092
4.7	1749.3	-28.4	174.7	7.2	0.4594
4.75	1763.4	-18.9	31.8	6.7	0.258
4.85	1791.6	10.4	32.4	14	0.7306
5.05	1847.9	-11.9	92.1	3.3	0.3147
5.1	1862.0	-34.2	152.7	6.7	0.235
5.2	1890.1	-13.5	46.3	11.6	0.2211
5.3	1918.3	-0.6	151.3	9.4	0.2882
5.35	1932.4	-7.7	87.5	8.8	0.4489
5.4	1946.5	-13	123.6	12.1	0.4392
5.45	1960.5	5.7	103	2.7	0.6689
5.5	1974.6	-6.2	145.3	8.6	0.4559
5.55	1988.7	12.2	78.2	8.8	0.3586
5.75	2045.0	-13.9	82.7	8.2	0.4016
5.8	2059.1	-48.1	-14	4.2	0.2469

5.85	2073.2	-25.9	39.1	8.4	0.2181
5.9	2087.3	-20.7	98.1	1.8	0.2282
5.95	2101.4	-30.8	35.8	8.7	0.0971
6.2	2171.8	-8.5	170.1	4.3	0.3108
6.25	2185.9	10.9	-29.7	2.7	0.4838
6.3	2199.9	-8	184.2	5.3	0.2075
6.35	2214.0	1.3	94.1	2.2	0.3299
6.45	2242.2	-12.5	32.6	5.1	0.2684
6.5	2256.3	-0.1	119.7	4	0.2287
6.6	2284.4	-28.8	90.6	3.7	0.2673
6.65	2298.5	15.9	175.2	7.4	0.251
6.7	2312.6	4.6	130.6	7.9	0.2748
6.8	2340.8	11.8	-23.4	2.7	0.2745
6.9	2368.9	4.4	-1.6	4.9	0.2881
7.05	2411.2	18.5	220.5	14.3	0.1597
7.1	2425.3	-9.6	103.4	14.3	0.3037
7.45	2523.8	2.2	-42.5	8.1	0.2324
7.6	2587.7	11.6	27.7	5	0.3134
7.65	2623.5	-9.5	-57.8	13.4	0.1547
7.85	2766.5	-17.6	-31.4	4	0.1943
7.9	2802.2	-12.9	-12.5	1.3	0.1429
8	2873.7	-14.9	-28.8	6.6	0.4429
8.05	2909.5	8.7	20.4	11.9	0.2848
8.1	2945.2	-12.6	-30.3	2.8	0.4131
8.15	2981.0	-9.8	-22	10.9	0.4767
8.2	3016.7	-9.8	-22	10.9	0.2594
8.25	3052.5	-34.6	30.6	6	0.1383
8.3	3088.2	-4.2	9.3	6.1	0.3062
8.35	3124.0	-18.1	142.7	5.9	0.1638
8.45	3195.5	26.3	119.8	6.6	0.3899
8.5	3231.2	-7.1	65.2	10.9	0.4138
8.6	3302.7	14.6	133.5	19	0.5229
8.75	3409.9	-5.5	216.8	14.1	0.3028
8.8	3445.7	-2.1	135.9	4.8	0.08
8.85	3481.4	16.1	37.1	12.5	0.479
8.9	3517.2	-5.2	151.7	1.9	0.117
9.2	3724.1	44.2	110.2	6.8	0.2196
9.25	3757.3	5.8	61.6	5.6	0.5183
9.3	3790.4	14.7	92.1	10.9	0.716
9.4	3856.7	14.5	105.4	8.5	0.3728
9.5	3923.0	37.7	100.4	12.8	0.5699
9.55	3956.1	3.5	115.5	13.7	0.6599
9.7	4055.6	30.2	171.9	3	0.1042
9.75	4088.7	25.7	128.5	2.2	0.5102

9.8	4121.8	-19.7	89.8	14.6	0.9072
9.85	4155.0	-4.7	179.1	3.7	0.5701
9.9	4188.1	46.9	92.7	16.8	0.4214
10	4254.4	5.4	198.5	2	0.3864
10.05	4287.6	1.9	189.2	15.5	0.6542
10.1	4320.7	-5.3	166.9	9.7	0.5332
10.15	4353.8	2.2	78.7	5.5	0.4606
10.25	4420.1	-33.1	123.5	10.9	0.2351
10.3	4453.3	-6.4	179.1	2.1	0.3572
10.4	4519.6	-37.5	159.8	9.6	0.4639
10.45	4552.7	25.8	183.1	10.9	0.2439
10.7	4743.5	-38.4	30	13.1	0.3918
10.8	4826.5	11.3	5.2	9.3	0.1591
10.95	4951.0	-33.6	49.3	3.3	0.1988
11	4992.5	16.1	51.3	26	0.3863
11.05	5034.0	-2.4	67.1	15.6	0.2363
11.15	5116.9	10.2	-30.6	23.2	0.1428
11.4	5324.4	-4.3	-54.2	9.8	0.1214
11.45	5365.9	13.4	8.6	5.5	0.4675
11.5	5407.4	13.1	8	16.2	0.6483
11.55	5448.9	34.1	-2.5	13	0.42
11.65	5531.9	41.1	3.5	9.3	0.1114
11.75	5614.9	15.9	54.9	7.6	0.2861
11.8	5656.4	0.2	9.4	14.8	0.3175
11.85	5697.9	-2.3	74.6	10.1	0.378
11.95	5780.9	-1.6	104.3	24.5	0.2811
12.25	6192.5	57.6	130.8	6.1	0.3072
12.3	6275.7	70.6	76.8	10	0.4276
12.4	6442.2	27.7	105.7	16.6	0.2471
12.5	6608.6	49.8	160.1	12.6	0.0998
12.55	6691.8	8.5	140.4	10.2	0.21
12.6	6775.0	19.5	59.5	2.8	0.2967
12.65	6858.2	69.1	266	7.9	0.4976
12.7	6941.4	5.5	142.6	9.3	0.3099
12.75	7024.6	59.4	166	9.7	0.1961
12.8	7107.8	-42	237.7	3.1	0.2372
12.9	7274.3	5.8	78.2	0.2	0.0544
12.95	7357.5	-46	200.1	2.9	0.3613
13	7440.7	5.3	182.3	14	0.2912
13.05	7523.9	28.7	106.5	2.4	0.2789
13.15	7690.3	-22.7	287.8	5.7	0.1176
13.2	7773.5	-13.2	172.2	2.9	0.2168
13.25	7856.7	-25.9	-12.1	6.9	0.1456
13.3	7939.9	13.7	64.6	9.7	0.176

13.35	8023.2	9.7	108.4	5.5	0.1837
13.4	8106.4	11.3	226.3	10.4	0.2427

		MD161/13		
Depth in m	Interpolated age	Inc° (15mT)	Relative	RPI 15mT
	in cal Yr BP		Dec° (15mT)	
1.72	459.9	-3	-46.6	5.105
1.76	465.4	-25.3	6.5	4.1478
1.8	470.8	-7.3	8	4.6723
1.86	479.0	-37.4	-38	5.4548
1.9	484.4	-3.6	-12.7	4.6999
1.92	487.1	-21.8	-39.3	4.5556
1.94	489.8	-6.3	-13.2	5.5828
1.96	492.6	-9.8	-1	5.8494
2.06	506.2	4.4	-10	6.3471
2.08	508.9	5	-5.2	5.2547
2.1	511.6	2.2	-17.3	4.2115
2.14	517.0	-9.5	-21.8	6.0251
2.16	519.8	0.3	-22.2	4.5052
2.18	522.5	4.2	-10.6	6.0408
2.2	525.2	12.4	-21.6	5.5643
2.28	536.1	-17.2	-22	8.6074
2.38	549.7	-26.2	-18.6	7.4529
2.4	552.4	-19.6	-11.5	8.3135
2.42	555.1	-23.1	-22.3	7.3115
2.44	557.8	-6.8	-9.2	8.0973
2.46	560.6	-13.4	-21.7	6.5671
2.48	563.3	-9.4	-2.1	8.2591
2.56	574.2	-6.9	-26.3	7.4543
2.66	587.8	-22.8	-17.6	7.7941
2.68	590.5	6.5	10.1	6.7748
2.74	598.6	-13.8	-13.2	7.2381
2.76	601.4	-28.8	-22.5	7.8486
2.78	604.1	-21.9	-33.6	8.3711
2.8	606.8	0.9	-46	6.7338
2.82	609.5	-9.1	-29.1	5.3671
2.86	615.0	-23.4	-18	5.6273
2.92	623.1	-11.2	-16.5	4.4815
2.94	625.8	-17.1	-5.7	4.1095
2.96	628.6	-6.3	-10.2	7.1261
2.98	631.3	-5.5	-23.9	7.3342

3	634.0	-31.2	-38.2	4.5588
3.22	663.9	-11.7	-36.3	5.927
3.24	666.6	-4.5	-6.8	5.2279
3.26	669.4	-11.7	0	4.6563
3.28	672.1	-8	-7.9	4.8351
3.3	674.8	-10.5	-7.3	4.6244
3.34	680.2	-10.6	-9.9	4.4505
3.36	683.0	-6.7	-24.4	8.2282
3.38	685.7	1.1	-2.5	7.1507
3.42	691.1	11	-4.4	5.9698
3.44	693.8	9.3	1.1	7.1365
3.46	696.6	6.4	-9.6	9.7552
3.6	715.6	3.8	-11.9	7.2517
3.64	721.0	8.5	-13.4	6.8846
3.68	726.5	5	0.2	4.6155
3.7	729.2	1.1	-16.5	5.5698
3.72	731.9	-8.8	-8.8	6.0297
3.76	737.4	-2.2	-31.8	6.8941
3.78	740.1	2.6	-24.4	5.6617
3.82	745.5	0.3	-20.9	5.2955
3.84	748.2	-11.8	-5.7	6.2068
3.86	751.0	6.7	-9	6.2396
3.88	753.7	15.1	-24	6.4003
3.9	756.4	11.7	-30.9	7.0989
3.92	759.1	-13.3	-11.6	7.3361
3.94	761.8	-3.5	-37.6	6.5944
3.96	764.6	2.2	-18.9	6.642
3.98	767.3	-2.6	-38.7	6.7177
4	770.0	18.2	5.6	6.0448
4.02	772.6	2.4	-24	6.3986
4.06	777.8	9.9	-24.5	7.5887
4.08	780.4	2.6	-39.7	6.8523
4.12	785.6	-14.4	-18.5	7.2283
4.16	790.8	-6	-25.1	6.4215
4.2	796.0	-14	-24.4	6.6189
4.22	798.6	0.1	-20	6.5959
4.24	801.2	-0.8	-12.1	7.0917
4.3	809.0	-0.8	-36.4	6.5741
4.32	811.6	4.7	-35	7.086
4.34	814.2	-2.1	-31.6	7.7836
4.38	819.4	-3	-27.5	6.134
4.4	822.0	5.6	-35.9	6.1673
4.42	824.6	4.4	-47.5	7.1617
4.48	832.4	1.2	-37.6	6.6912

4.78	871.4	3.8	-28.1	8.0356
4.82	876.6	-13	-25	7.4647
4.84	879.2	-3.5	-40.6	6.8626
4.86	881.8	0.3	-36.2	6.9545
4.92	889.6	-8.2	-25.1	5.7603
5.02	902.6	11.1	-46	5.1968
5.06	907.8	5.2	-11	5.6592
5.08	910.4	-12	-21.6	4.8772
5.1	913.0	3.3	-49.8	5.9797
5.12	915.6	7.3	-46.4	5.6969
5.14	918.2	11.1	-47.4	6.2295
5.18	923.4	9.8	-49.3	5.5127
5.22	928.6	4.9	-34	5.9273
5.28	936.4	4.3	-44.5	5.5844
5.44	957.2	37.5	-39.2	6.445
5.46	959.8	22.1	-45.4	5.5828
5.5	965.0	11.1	-32.7	5.4949
5.54	970.2	8.2	-47.8	5.9132
5.56	972.8	27.4	-34.3	4.5473
5.58	975.4	15.7	-36.2	4.9205
5.62	980.6	27.7	-48.2	5.5173
5.64	983.2	25.1	-49.3	5.189
5.66	985.8	21.3	-27	5.2056
5.74	996.2	7.3	-39.4	5.78
5.76	998.8	13.4	-45.1	6.5199
5.82	1006.6	18	-40.4	5.519
5.84	1009.2	3.4	-31.1	5.8347
5.86	1011.8	11.5	-40	4.7403
5.9	1017.0	2.9	-45.3	6.1653
5.92	1019.6	16.7	-49.3	5.4392
5.94	1022.2	27.2	-49.1	6.0595
5.96	1024.8	11.7	-47.3	5.8066
6	1030.0	6	-49.2	6.1542
6.22	1058.6	-4.2	-49.2	5.8412
6.24	1061.2	7.8	-40.7	6.5229
6.3	1069.0	3.7	-25	5.606
6.34	1074.2	6.4	-45.8	6.4635
6.36	1076.8	-2	-46.5	6.8629
6.38	1079.4	-4.8	-31.5	6.9818
6.4	1082.0	9.2	-38.6	6.385
6.46	1089.8	18.8	-32.5	5.9946
6.48	1092.4	2.5	-43.2	7.1431
6.5	1095.0	4.5	-25.2	6.7019
6.52	1097.6	8.2	-24.9	6.3521

6.54	1100.2	4.2	-23	5.7025
6.56	1102.8	4.4	-34.9	6.0981
6.58	1105.4	3.8	-36.2	5.3691
6.6	1108.0	9.5	-26	5.3834
6.62	1110.6	-1.2	-36.9	6.0293
6.66	1115.8	7.7	-49	6.8632
6.68	1118.4	7.9	-23.6	6.1657
6.72	1123.6	7.5	-35.3	6.6453
6.76	1128.8	3.3	-47.4	5.6074
6.78	1131.4	1.8	-40.6	5.6048
6.8	1134.0	5	-34.9	6.0787
6.82	1136.6	-3.1	-34.1	5.8
6.84	1139.2	1.5	-24	5.9684
6.9	1147.0	3.3	-41.8	5.6678
6.92	1149.6	13.2	-33.5	5.4032
6.94	1152.2	19	-27.7	5.4364
7	1160.0	7.5	-24.4	5.8373
7.04	1165.2	12.9	-49.1	5.1403
7.06	1167.8	15.4	-15.8	5.6804
7.08	1170.4	28.2	-29.5	5.6238
7.12	1175.6	-2.9	-43.3	5.328
7.2	1186.0	15.5	-43.1	5.8887
7.24	1191.2	25.7	-33.4	6.1826
7.26	1193.8	1.3	-37.5	5.1069
7.3	1199.0	15.5	-44.4	6.4769
7.36	1206.8	22.2	-42	4.3479
7.4	1212.0	6.4	-46.1	5.2878
7.42	1214.6	14.8	-41.4	6.6278
7.46	1219.8	12.3	-35.9	6.4155
7.48	1222.4	8.2	-38.4	7.0428
7.5	1225.0	4.4	-36.9	6.7264
7.64	1243.2	5.1	-28.6	5.5944
7.68	1248.4	15.2	-29.4	5.5892
7.7	1251.0	31.1	-30.1	7.111
7.72	1253.6	31.6	-28.4	6.2356
7.76	1258.8	6.7	-5.6	6.2892
7.8	1264.0	11.9	-3.7	5.8769
7.88	1274.4	22.5	-35.5	6.0148
7.9	1277.0	20.7	-29.3	6.5136
7.94	1282.2	30.4	-28.5	5.8394
7.96	1284.8	19.5	-28.4	5.8358
7.98	1287.4	13.3	-22.6	6.8864
8	1290.0	18.7	-9.1	6.2415
8.02	1292.6	39.8	-23.3	6.0382

8.04	1295.2	19.5	-40.1	5.4592
8.08	1300.4	18.1	-48.8	5.9135
8.1	1303.0	20.5	-26.5	6.7887
8.14	1308.2	24.4	-32.6	7.0313
8.2	1316.0	19.6	-18.4	7.4101
8.22	1318.6	20.5	-20	6.0878
8.24	1321.2	38.8	-30.9	5.5045
8.26	1323.8	36.6	-13.1	6
8.28	1326.4	42.9	-23	6.333
8.32	1331.6	14.2	-40.1	7.7432
8.36	1336.8	39.8	-29	6.6413
8.38	1339.4	48.7	-21.4	6.6975
8.4	1342.0	37	-4	6.7314
8.44	1347.2	44	-8	5.9445
8.5	1355.0	32.9	-13.1	6.7229
8.52	1357.6	33.4	12.1	6.2897
8.54	1360.2	36.7	10.2	8.1439
8.56	1362.8	44.5	-0.9	8.0496
8.58	1365.4	39.4	9.9	8.2547
8.6	1368.0	44.9	11.3	6.4763
8.62	1370.6	20.6	5	6.6047
8.64	1373.2	29.9	10.4	7.4647
8.66	1375.8	26.4	-16.5	8.0324
8.68	1378.4	19.6	10.6	8.2799
8.7	1381.0	25.1	-14.5	8.6492
8.74	1386.2	42	-27.1	6.9886
8.76	1388.8	19.2	-9.7	6.7494
8.78	1391.4	25.2	2.3	6.8102
8.82	1396.6	27.3	-15.9	6.9689
8.86	1401.8	32.5	-17.6	6.9803
8.88	1404.4	30.5	-5.6	6.8631
8.92	1409.6	30.1	-16.5	7.0847
9.24	1466.8	10.1	-29	7.0274
9.26	1470.7	9.5	-17.6	6.584
9.28	1474.6	20.8	-26	6.6157
9.32	1482.4	16.2	-26.1	8.2742
9.36	1490.2	18	-7.3	7.1014
9.38	1494.1	7.3	-18.4	7.1008
9.4	1498.0	11.6	-18.7	7.6153
9.42	1501.9	4.5	-14.6	7.0491
9.44	1505.8	9.8	-26.1	6.3426
9.46	1509.7	8.4	-23.7	6.2814
9.48	1513.6	5.4	-16.5	6.7196
9.5	1517.5	10.6	-18.9	6.7077

9.52	1521.4	11.6	-37.8	6.4857
9.54	1525.3	12.3	-28.9	6.4235
9.56	1529.2	4.7	-27.9	5.6663
9.58	1533.1	11.1	-28.1	6.3418
9.6	1537.0	12.1	-27.7	5.5378
9.68	1552.6	8.9	-22.8	7.0552
9.7	1556.5	6.8	-19.6	6.56
9.72	1560.4	11.9	-17.3	7.496
9.76	1568.2	10.6	-20.4	6.167
9.8	1576.0	4	-27.8	5.7623
9.82	1579.9	2.9	-23.5	6.0589
9.84	1583.8	6.7	-21.9	6.7012
9.86	1587.7	6.8	-19.7	6.9998
9.88	1591.6	12.1	-4.1	6.5969
9.9	1595.5	11.3	-6.1	6.2525
9.96	1607.2	7.9	-19.1	4.9108
9.98	1611.1	9.2	-16.6	6.3469
10	1615.0	6.4	-24.9	6.1197
10.02	1618.9	12.9	-16	5.9755
10.06	1626.7	13.8	-17.2	5.4288
10.08	1630.6	18.8	-19.1	5.9257
10.1	1634.5	18.9	-6.3	6.8383
10.12	1638.4	14.1	-25.8	4.6076
10.14	1642.3	11.3	-15.7	4.8621
10.16	1646.2	13	6.2	5.9102
10.18	1650.1	14	-6.1	5.6207
10.2	1654.0	7.1	1.7	5.4146
10.22	1657.9	6.6	-2	5.7615
10.24	1661.8	14.2	3.9	5.7251
10.26	1665.7	-12.4	-8.3	6.4415
10.28	1669.6	-10.8	0.6	7.0768
10.3	1673.5	-13.2	-14.2	7.0023
10.32	1677.4	-10.3	-1.5	6.3729
10.34	1681.3	2.4	-4.3	6.0897
10.36	1685.2	3.7	-15.7	6.6614
10.38	1689.1	0.8	11.1	6.4781
10.4	1693.0	9.2	21.2	6.9841
10.42	1696.9	0.5	5.3	7.2864
10.44	1700.8	5.6	7.9	7.6039
10.46	1704.7	3	-6.1	6.2853
10.5	1712.5	5.5	12.8	6.64
10.52	1716.4	1.6	-5.2	6.6048
10.64	1739.8	0.2	13.2	6.5033
10.7	1751.5	-1.8	14.1	6.1277

10.72	1755.4	-2.4	13.8	6.5648
10.78	1767.1	-4.6	7.5	6.7519
10.8	1771.0	5	18.9	6.5354
10.82	1774.9	5.3	10.2	6.6831
10.84	1778.8	7.5	20.1	6.7057
10.86	1782.7	2.1	15.1	6.7321
10.92	1794.4	12.3	16.7	7.8617
10.94	1798.3	7.8	13.4	7.6562
10.96	1802.2	4.1	12.5	6.9572
11	1810.0	9.7	7.3	7.6564
11.02	1813.9	-4.2	29	7.9694
11.04	1817.8	5.7	27.6	6.1646
11.06	1821.7	4.7	15.5	5.7346
11.08	1825.6	2.5	31	5.757
11.1	1829.5	9.6	20.9	5.6082
11.12	1833.4	0.1	21.5	6.7956
11.16	1841.2	6.8	25	6.4581
11.18	1845.1	3	27.4	6.2299
11.2	1849.0	2.8	14.2	5.9183
11.22	1852.9	5.4	5.8	6.4735
11.24	1856.8	-1.5	16.6	6.6084
11.26	1860.7	1.3	20.1	6.1197
11.28	1864.6	-1.5	28.3	6.2514
11.3	1868.5	1	18.4	7.0031
11.32	1872.4	5.5	19.5	7.4139
11.34	1876.3	7.4	6.3	6.2222
11.36	1880.2	-3.9	1.9	6.2565
11.4	1888.0	-8	17	5.9172
11.42	1893.2	-4.6	9.7	5.9925
11.46	1898.3	-6.7	-1.5	6.1111
11.48	1900.9	-5.9	20.2	6.1195
11.5	1903.5	-9.9	0.4	6.1265
11.52	1906.1	-4	1.5	6.7148
11.54	1908.7	-3	14	6.6294
11.56	1911.2	-6.4	16.1	6.0898
11.58	1913.8	-5.6	7.6	6.9059
11.6	1916.4	-8.5	1.4	7.0297
11.62	1919.0	-11	20.7	6.4641
11.64	1921.6	-5.9	12.8	6.589
11.66	1924.1	3.5	16.7	7.4744
11.68	1926.7	-0.7	11.3	6.7225
11.7	1929.3	-8.2	22	7.709
11.72	1931.9	-5.6	14.3	7.1296
11.74	1934.5	-11.4	15	7.1464

11.78	1939.6	-13	15	5.833
11.82	1944.8	-1.3	35.2	6.23
11.84	1947.4	-4.1	20.2	6.5464
11.86	1949.9	1.7	33.9	5.0932
11.88	1952.5	-4.5	9.8	6.6134
11.9	1955.1	2.6	3	5.4977
11.92	1957.7	0.8	15	6.1369
11.94	1960.3	-3.4	14.7	7.0244
11.98	1965.4	-2	18.2	7.1631
12	1968.0	-4.5	13.9	8.5387
12.22	1996.4	11.9	44.4	8.7455
12.24	1999.0	-9.2	47.8	6.0488
12.28	2004.1	1.3	35.9	5.6989
12.3	2006.7	-8.6	42.8	6.1045
12.32	2009.3	-2.2	33	6.0188
12.34	2011.9	-14.9	30.6	6.2334
12.38	2017.0	-1.3	43.1	5.9447
12.4	2019.6	-1.3	40.9	6.3802
12.42	2022.2	-6.3	46.8	5.7969
12.44	2024.8	-9.5	45.1	5.9628
12.46	2027.3	-13.4	49.7	5.8288
12.48	2029.9	6.2	33.6	6.202
12.52	2035.1	-3.5	44.5	6.3724
12.54	2037.7	1.2	41.3	6.295
12.56	2040.2	-4.4	48.9	6.6221
12.58	2042.8	2.2	52.1	6.705
12.6	2045.4	3.1	24.7	6.2782
12.62	2048.0	-3.6	55.7	5.404
12.66	2053.1	-3.3	56.2	5.0003
12.68	2055.7	-9.3	68.5	5.7594
12.7	2058.3	-2.9	40.7	5.0102
12.74	2063.5	-6.5	53.5	5.3328
12.76	2066.0	6	60.6	5.7519
12.8	2071.2	-5	48.5	6.0411
12.82	2073.8	-6.5	40.8	6.5964
12.84	2076.4	-5.4	51.2	5.9172
12.9	2084.1	2.5	40.5	6.6751
12.92	2086.7	-3.6	37.2	5.8156
12.94	2089.3	-2.7	32.1	5.8212
12.96	2091.8	-0.4	34	5.7728
12.98	2094.4	-4	47.8	5.6243
13	2097.0	-11.4	57	5.3878
13.02	2099.6	-5.5	46.4	5.8323
13.04	2102.2	-16.9	44.3	6.7904

13.08	2107.3	-8.6	43.6	4.964
13.12	2112.5	-7.3	43.9	5.5803
13.14	2115.1	-15.6	51.2	5.9422
13.16	2117.6	-14.2	56.5	5.9301
13.18	2120.2	-25.5	55.1	6.4746
13.2	2122.8	-18.2	45.9	6.395
13.24	2128.0	-21.4	50.6	5.7074
13.26	2130.5	-20.8	62.9	4.6704
13.28	2133.1	-13	42	5.5138
13.3	2135.7	-27.1	51.3	5.4068
13.32	2138.3	-10.6	41.2	5.6972
13.34	2140.9	-22.7	55.1	5.6064
13.36	2143.4	-21	51.4	4.9291
13.4	2148.6	-10.8	39.2	5.125
13.42	2151.2	-9.4	42.8	5.2287
13.44	2153.8	-17.9	47.6	5.7376
13.46	2156.3	-8.7	46.2	4.6122
13.62	2177.0	6.8	47	5.893
13.64	2179.6	7.6	57.3	7.0169
13.66	2182.1	12.4	43.9	7.5743
13.68	2184.7	4.4	41.7	7.5335
13.7	2187.3	11.7	43.3	6.9069
13.72	2189.9	9.6	42.1	6.7853
13.74	2192.5	5.9	43.3	6.3189
13.76	2195.0	2	40.3	5.3152
13.78	2197.6	1.6	40.8	5.6146
13.82	2209.4	10.1	52.7	6.4749
13.84	2214.6	8.6	39.2	6.3039
13.88	2224.9	2	40.3	5.1501
13.9	2230.1	7.5	45.6	5.5616
13.92	2235.3	5.7	48.6	5.752
13.94	2240.5	6.4	41.1	6.2568
13.98	2250.8	9	45.5	6.0525
14	2256.0	19.1	33.1	6.5488
14.02	2261.2	4.7	43.9	6.9138
14.06	2271.5	10.3	34	6.2569
14.1	2281.9	11	37	5.8828
14.12	2287.1	9.2	39	5.6728
14.16	2297.4	19.8	29.7	6.0214
14.18	2302.6	7.9	45.5	5.618
14.24	2318.2	14.5	24.1	5.2598
14.28	2328.5	15.9	29.3	6.5276
14.3	2333.7	9.7	40.4	5.4447
14.32	2338.9	16.3	34.6	5.4139

14.34	2344.1	17.4	54.6	6.0061
14.38	2354.4	16.8	50.8	5.9077
14.4	2359.6	14.3	43.7	5.1049
14.46	2375.1	11.2	43.6	6.3199
14.48	2380.3	13.9	40.8	6.0934
14.5	2385.5	19.1	55.5	6.194
14.52	2390.7	18.1	44.9	5.7954
14.54	2395.9	25.4	52.9	5.8124
14.56	2401.0	20.3	50.2	6.9537
14.6	2411.4	16.9	48.6	5.6605
14.62	2416.6	16.8	40.2	5.0972
14.64	2421.8	19.3	61.2	4.5342
14.66	2426.9	17	57.9	5.0762
14.68	2432.1	12	52.1	5.5076
14.72	2442.5	15.3	59.2	4.5576
14.74	2447.7	15	44.2	3.6159
14.8	2463.2	12.1	50.4	4.8397
14.82	2468.4	19.1	46	6.157
14.86	2478.7	13	55.7	5.4849
14.9	2489.1	18.7	44.1	6.0391
14.96	2504.6	18.1	49.1	6.3888
15	2515.0	10.4	53.9	5.5044
15.22	2572.0	5.3	35.6	5.8846
15.24	2577.2	4.1	39.2	6.7892
15.26	2582.3	7.3	26.2	6.9564
15.28	2587.5	6.6	33.6	6.5161
15.3	2592.7	8.7	21.3	7.072
15.34	2603.1	7.2	21.2	7.2928
15.36	2608.2	7.1	20.8	7.2506
15.38	2613.4	8.7	33.4	6.4526
15.4	2618.6	12.5	22.6	7.1531
15.42	2623.8	9.5	33.2	7.0423
15.44	2629.0	10.8	37.4	6.74
15.46	2634.1	12.5	37.8	5.421
15.48	2639.3	11.9	36	5.3758
15.5	2644.5	15.9	26.3	5.7213
15.52	2649.7	12	23.3	5.5518
15.54	2654.9	6.5	23.3	6.3896
15.56	2660.0	12.8	37	6.6616
15.58	2665.2	19.4	19	6.9778
15.6	2670.4	13.2	25.2	7.6301
15.62	2675.6	16	35.1	7.3081
15.66	2685.9	11.5	36.6	6.8598
15.68	2691.1	13.2	24	6.0962

15.7	2696.3	13.3	30	6.6111
15.72	2701.5	12.1	27.9	6.9238
15.74	2706.7	12.4	20.9	6.9002
15.76	2711.8	11.2	26.2	7.2762
15.78	2717.0	14	31.1	6.9397
15.8	2722.2	16.4	48.1	7.3661
15.82	2727.4	13.2	30.8	7.4823
15.84	2732.6	13.6	36.5	6.8587
15.86	2737.7	18.6	32.9	7.4203
15.9	2748.1	19.1	23.2	7.2469
15.94	2758.5	10.9	38.4	6.59
15.96	2763.6	2.5	39.3	6.4202
16.02	2774.0	12.6	35.1	6.251
16.04	2778.0	9.8	36.7	6.151
16.06	2782.0	11.3	45.2	6.6807
16.08	2786.0	16.1	39.7	6.7453
16.1	2790.0	14.1	41.1	6.8267
16.12	2794.0	12	37.3	7.8122
16.14	2798.0	14.7	22.9	6.5965
16.16	2802.0	9.2	51	7.0744
16.18	2806.0	2.8	32.8	6.9233
16.2	2810.0	9	32	7.0979
16.22	2814.0	9.1	28.7	6.637
16.26	2822.0	-0.2	41.6	6.4265
16.28	2826.0	4.8	38.3	5.9692
16.3	2830.0	5.9	29.4	6.788
16.32	2834.0	2.7	45.7	6.9508
16.34	2838.0	1.9	40	6.1017
16.36	2842.0	0.2	37.7	6.967
16.38	2846.0	8	47	7.8025
16.4	2850.0	5.3	38.4	7.5716
16.42	2854.0	3.1	52.4	7.4327
16.44	2858.0	0.1	46.6	7.3548
16.68	2906.0	5.1	-1.8	7.0531
16.7	2910.0	0.5	-8.2	5.2483
16.72	2914.0	24.8	-1.5	6.5984
16.86	2942.0	18.8	20.3	7.3555
16.88	2946.0	21.5	-19.8	6.751
16.92	2954.0	13.9	4.4	7.2032
16.94	2958.0	11.1	-14.9	6.1871
16.98	2966.0	6.7	-1	7.469
17	2970.0	1.9	16.8	7.1747
17.02	2974.0	32.4	12.5	8.1573
17.08	2986.0	16.6	29.4	8.0167

17.1	2990.0	7	-11.5	9.7124
17.14	2998.0	25	0.2	8.0547
17.16	3002.0	7	5.5	6.4276
17.18	3006.0	17	1.8	5.7178
17.2	3010.0	14.7	13.8	8.9427
17.22	3014.0	5.3	19.9	5.6605
17.26	3022.0	22.9	22	6.1429
17.28	3026.0	11.6	6.7	6.1189
17.3	3030.0	13.9	4.5	5.6098
17.36	3042.0	23.4	24.4	5.9574
17.38	3046.0	13.1	22.1	5.9066
17.4	3050.0	18.5	7.2	6.1691
17.44	3058.0	12.5	7.3	5.3629
17.5	3070.0	16.3	-24.7	5.8467
17.52	3074.0	0.5	-4.2	5.6851
17.54	3078.0	12.2	16	4.3647
17.56	3082.0	5.8	10.1	5.9288
17.64	3098.0	10	16.3	7.7488
17.66	3102.0	8	-0.4	7.4096
17.68	3106.0	13.4	-12.5	6.8101
17.76	3122.0	15.9	9.5	4.9644
17.82	3134.0	24.4	9.6	5.8179
17.84	3138.0	14	-7.8	7.7004
17.86	3142.0	18.6	18.7	6.2279
18.24	3218.0	-0.8	6.1	5.3108
18.26	3222.0	10.7	11.9	6.0064
18.3	3230.0	2.3	17.7	7.1975
18.32	3234.0	4	13.7	6.0232
18.36	3242.0	-2.1	33.5	4.6858
18.4	3250.0	7.6	34.2	5.2053
18.42	3254.9	-8.5	26.6	6.099
18.44	3259.0	-2.2	6.8	7.0679
18.46	3263.1	-2.4	-2.3	6.6837
18.48	3267.1	-6.7	14.4	6.5132
18.5	3271.2	4.3	10.7	5.7833
18.54	3279.4	16.7	37.9	5.4344
18.58	3287.5	14.8	23.6	5.2996
18.6	3291.6	2	2.4	5.444
18.62	3295.7	5.4	-1.7	7.213
18.64	3299.8	3.3	23.9	7.1644
18.68	3307.9	-2.4	10.9	6.2815
18.7	3312.0	-2.2	0.9	8.5957
18.72	3316.1	-1.4	16.2	7.627
18.8	3332.4	-4.8	19.9	5.7327

18.82	3336.5	-2.6	18.8	5.0544
18.92	3356.8	-1.4	27.7	7.4981
18.94	3360.9	8.9	-0.1	6.6592
18.96	3365.0	1.4	-2.8	5.8461
19.08	3389.5	-2.3	25.7	4.5659
19.1	3393.5	-6.3	35.3	4.6657
19.14	3401.7	6.8	19.4	5.0492
19.16	3405.8	-2.8	9.7	5.957
19.18	3409.8	-3.3	23.4	6.6255
19.2	3413.9	-0.9	12.7	6.4787
19.22	3418.0	6.6	15.9	7.0881
19.24	3422.1	-0.6	25.5	6.303
19.26	3426.2	-1.4	9.8	4.463
19.28	3430.2	7.7	14.1	4.4022
19.32	3438.4	2.6	16.9	5.018
19.36	3446.5	15.8	6.9	5.2106
19.38	3450.6	7.2	27.3	5.1417
19.42	3458.8	-10.1	18.8	4.1132
19.44	3462.8	8.3	19.6	5.2803
19.46	3466.9	8.9	4	5.5254
19.5	3475.1	-12.1	5.4	5.7877
19.62	3499.5	10.3	14.5	4.9741
19.64	3503.6	10.8	22.8	5.0909
19.66	3507.7	16.8	21.5	5.1105
19.68	3511.8	11.8	24.8	6.4512
19.7	3515.8	2.7	29.1	6.0429
19.74	3524.0	3.4	26.2	5.6428
19.76	3528.1	12.4	23.8	3.9733
19.78	3532.2	8.4	18.4	4.9151
19.8	3536.2	-2.9	21	5.9534
19.82	3540.3	-0.3	25.3	5.4764
19.84	3544.4	10.7	17.3	4.8029
19.86	3548.5	17	33.5	4.3603
19.88	3552.5	5.1	28.8	4.6274
19.9	3556.6	9	37.7	5.5187
19.92	3560.7	10.7	33.1	5.8321
19.94	3564.8	20.3	35.3	4.6792
19.96	3568.8	11.8	15.5	4.9217
20	3577.0	6.4	26.5	4.5794
20.02	3581.1	5.1	27.1	4.8825
20.04	3585.2	6.5	20.6	5.0255
20.06	3589.2	5.9	33.1	4.3952
20.08	3593.3	-4	22.3	5.4209
20.1	3597.4	-5	29.8	6.5585

20.12	3601.5	15.9	34.4	6.3622
20.14	3605.5	22.7	15.7	4.9589
20.16	3609.6	27.1	34.4	4.4389
20.18	3613.7	12.4	15.6	5.8825
20.2	3617.8	-4	58.5	6.0937
20.22	3621.8	-2.6	60.4	5.6076
20.24	3625.9	3.3	64.2	5.2612
20.28	3634.1	0.7	35.8	5.1233
20.3	3638.2	26.4	-5.3	4.2159
20.32	3642.2	23.1	-3.2	4.48
20.38	3654.5	22.4	26.6	4.9564
20.4	3658.5	27.1	37.9	4.0382
20.42	3662.6	27.2	19.8	4.5293
20.44	3666.7	20.1	47	4.9893
20.46	3670.8	20.1	38.1	4.5332
20.48	3674.8	15.6	1.6	3.9548
20.5	3678.9	31.9	25	4.1583
20.52	3683.0	20.3	26.7	5.936
20.54	3687.1	12.3	24	6.2382
20.56	3691.2	5.5	5.3	5.3403
20.6	3699.3	18.1	9.4	6.4532
20.62	3703.4	12.9	58.4	5.1561
20.64	3707.5	15.8	-6.9	3.5732
20.66	3711.5	29.3	45.6	3.8262
20.68	3715.6	12.4	18.8	3.7815
20.72	3723.8	16.7	16	4.1235
20.74	3727.8	7.1	22.1	3.8491
20.76	3731.9	7	31.8	4.3836
20.78	3736.0	19.3	40	4.6142
20.8	3740.1	22.9	38.3	4.5569
20.82	3744.2	18.5	-1.7	5.2514
20.84	3748.2	26.6	6.5	4.7772
20.86	3752.3	20.9	32.3	7.3715
20.88	3756.4	-17.3	13.5	4.7231
20.9	3760.5	-6.6	21.5	4.4173
21.22	3824.0	-3.6	12	5.4088
21.24	3828.0	1.4	42.4	4.3163
21.26	3832.0	-9.6	27.5	5.0684
21.28	3836.0	-9.5	25.3	4.2748
21.3	3840.0	-9.3	24.7	3.8128
21.32	3844.0	-7.6	30.9	3.5891
21.34	3848.0	-7.9	34.3	3.8399
21.38	3856.0	-19.3	24.8	4.4882
21.46	3872.0	-8.6	24	4.819

21.5	3880.0	-1.8	33.7	5.0709
21.52	3884.0	-8.1	42.2	4.3158
21.54	3888.0	-7.4	30.6	4.2842
21.56	3892.0	-2.2	39	4.3877
21.58	3896.0	-4.6	37	3.9947
21.6	3900.0	1.4	29.1	3.8813
21.62	3904.0	-2	26.1	4.6441
21.64	3908.0	2.4	41.2	5.2346
21.66	3912.0	2.9	29.2	5.777

Table 2. Variations in rock magnetic parameters of MD161/13.

Depth in m	Interpolated age	$\chi_{LF} \times 10^{-6}$	$\chi_{fd}\%$	$\chi_{ARM} \times 10^{-5}$	SIRM $\times 10^{-5}$	Soft IRM $\times 10^{-5}$	HIRM $\times 10^{-5}$	S-ratio
	in cal. Yr. BP	m3kg ⁻¹		m3kg ⁻¹	Am ² kg ⁻¹	Am ² kg ⁻¹	Am ² kg ⁻¹	
0.28	264.1	1.07	2.99	0.97	2023.93	806.77	70.73	0.933
0.38	277.7	1.16	2.36	0.97	2104.28	606.36	50.41	0.951
0.5	294.0	1.18	3.14	1.01	2251.46	826.54	34.03	0.970
0.66	315.8	1.32	3.39	0.91	2407.13	646.87	18.93	0.985
0.84	340.2	1.26	3.38	1.09	2287.00	898.19	58.37	0.947
0.98	359.3	1.16	3.01	1.05	2295.03	918.91	41.20	0.962
1.08	372.9	1.30	2.75	1.10	2581.95	1061.13	64.80	0.946
1.2	389.2	1.17	2.47	1.01	2203.91	986.79	44.74	0.960
1.36	411.0	1.00	4.06	0.98	1743.80	730.77	38.80	0.957
1.48	427.3	1.02	3.50	0.99	1868.36	830.85	40.27	0.958
1.78	468.1	1.05	3.09	0.95	2012.11	882.02	50.55	0.952
1.88	481.7	1.01	2.85	0.91	2029.44	928.16	28.81	0.972
1.98	495.3	1.33	2.46	0.99	2774.11	1251.78	56.94	0.959
2.08	508.9	1.26	3.19	1.00	2493.74	1119.02	60.43	0.954
2.18	522.5	1.09	3.69	0.96	2003.69	874.79	29.16	0.971
2.3	538.8	1.09	3.77	0.94	2030.86	896.31	72.05	0.930
2.4	552.4	1.04	4.26	1.00	1826.86	793.92	53.29	0.941
2.5	566.0	1.08	3.43	1.08	1980.98	854.29	66.13	0.935
2.6	579.6	1.20	3.42	1.15	2254.92	955.19	64.96	0.942
2.74	598.6	1.22	3.79	1.00	2174.08	933.63	86.08	0.923
2.84	612.2	1.00	3.48	0.96	1873.25	793.18	42.56	0.954
2.94	625.8	1.13	2.71	1.00	2147.67	905.01	57.33	0.945
3.24	666.6	0.99	3.47	0.96	1810.39	789.97	45.39	0.950
3.34	680.2	1.08	3.28	0.99	2073.56	900.87	83.49	0.918
3.44	693.8	1.22	3.27	0.98	2355.10	881.04	77.39	0.933
3.54	707.4	1.09	2.99	0.94	1990.81	827.67	78.44	0.921
3.64	721.0	1.09	3.08	0.96	1982.95	788.86	51.78	0.945
3.76	737.4	1.05	2.89	1.01	1882.15	747.12	47.19	0.950

3.88	753.7	1.12	2.62	0.99	2042.78	841.40	37.71	0.963
3.98	767.3	1.04	3.59	0.99	1880.17	710.58	44.26	0.953
4.08	780.4	1.24	3.25	0.97	2434.78	972.11	66.63	0.945
4.22	798.6	1.08	3.27	0.96	2022.56	823.89	64.93	0.934
4.32	811.6	1.08	3.23	0.90	2051.62	822.36	62.14	0.937
4.42	824.6	1.10	2.07	0.97	2092.64	808.69	71.34	0.928
4.72	863.6	1.20	3.69	0.97	2302.28	966.71	78.04	0.932
4.82	876.6	1.27	3.51	0.96	2406.98	975.39	66.55	0.945
4.92	889.6	1.09	4.07	0.99	2054.64	841.65	59.97	0.945
5.02	902.6	1.00	3.70	0.96	1831.69	703.47	55.47	0.940
5.12	915.6	0.98	4.22	0.91	1817.10	728.06	46.57	0.949
5.22	928.6	1.06	3.45	0.95	1987.80	827.93	67.12	0.932
5.32	941.6	1.25	2.66	0.99	2444.33	1005.84	43.90	0.963
5.42	954.6	1.14	2.73	0.91	2174.00	947.32	66.90	0.941
5.52	967.6	0.98	3.42	0.89	1742.20	737.25	28.00	0.967
5.62	980.6	0.92	3.19	0.86	1627.10	716.43	49.88	0.939
5.74	996.2	1.05	3.16	0.92	1805.30	746.99	41.67	0.955
5.84	1009.2	0.93	4.75	0.91	1628.58	725.76	51.03	0.939
5.94	1022.2	0.99	3.48	0.91	1716.25	714.67	58.59	0.932
6.24	1061.2	1.00	3.12	0.88	1748.08	686.51	43.78	0.950
6.36	1076.8	1.05	3.52	0.91	1830.38	746.91	31.31	0.966
6.46	1089.8	1.00	3.33	0.90	1787.82	751.81	54.59	0.940
6.56	1102.8	1.00	3.31	0.90	1712.52	727.67	45.16	0.947
6.66	1115.8	1.07	3.81	0.90	1829.37	734.30	38.43	0.959
6.76	1128.8	1.02	3.73	0.92	1769.06	722.73	61.25	0.931
6.86	1141.8	0.97	3.10	0.87	1680.96	633.05	38.29	0.955
6.98	1157.4	1.01	3.19	0.84	1808.83	750.55	59.56	0.936
7.08	1170.4	0.95	3.94	0.88	1644.03	715.73	53.19	0.935
7.22	1188.6	1.00	3.06	0.87	1800.76	749.24	49.23	0.946
7.32	1201.6	0.98	3.36	0.82	1727.60	700.11	64.95	0.924
7.44	1217.2	1.02	3.37	0.86	1840.07	759.51	49.37	0.946
7.64	1243.2	0.93	3.11	0.84	1587.94	626.16	56.15	0.931
7.74	1256.2	1.05	3.12	0.86	1926.14	803.86	43.78	0.956
7.86	1271.8	1.04	2.70	0.86	1898.53	822.35	31.10	0.965
7.96	1284.8	1.00	3.00	0.89	1815.41	777.99	40.98	0.955
8.06	1297.8	1.01	3.10	0.90	1839.72	764.11	49.90	0.944
8.18	1313.4	1.08	2.91	0.90	2014.91	902.86	46.50	0.953
8.28	1326.4	1.05	3.28	0.94	1915.28	846.25	58.84	0.938
8.4	1342.0	0.97	2.92	0.91	1714.88	764.35	49.88	0.941
8.5	1355.0	1.05	3.35	0.90	1920.31	829.37	49.35	0.949
8.6	1368.0	1.13	3.64	0.93	1963.36	866.41	48.31	0.950
8.7	1381.0	1.12	3.57	0.90	1974.75	865.21	43.11	0.956
8.8	1394.0	0.93	4.20	0.86	1575.30	687.33	49.02	0.938

8.92	1409.6	1.01	3.87	0.88	1776.67	771.25	80.56	0.912
9.24	1466.8	0.99	3.15	0.85	1737.60	759.08	44.29	0.949
9.34	1486.3	0.97	3.07	0.82	1746.29	778.54	63.83	0.930
9.44	1505.8	0.92	3.29	0.82	1589.16	737.54	47.94	0.940
9.54	1525.3	0.93	2.92	0.80	1612.08	733.76	35.74	0.956
9.64	1544.8	1.04	3.15	0.86	1816.58	789.57	34.68	0.962
9.76	1568.2	1.01	2.71	0.80	1747.06	813.51	46.31	0.947
9.86	1587.7	0.95	3.33	0.82	1603.77	733.33	26.35	0.967
9.98	1611.1	0.88	3.02	0.79	1518.38	723.32	36.70	0.952
10.08	1630.6	0.86	3.13	0.78	1491.90	672.82	57.22	0.925
10.18	1650.1	0.82	4.31	0.78	1405.86	656.26	35.93	0.949
10.28	1669.6	0.95	3.06	0.81	1714.68	788.24	39.99	0.955
10.38	1689.1	0.97	3.29	0.84	1759.11	834.66	48.20	0.946
10.48	1708.6	1.01	3.20	0.88	1810.53	800.29	47.29	0.949
10.68	1747.6	0.92	4.01	0.93	1623.15	671.50	66.05	0.920
10.78	1767.1	0.90	3.45	0.88	1601.86	715.95	50.88	0.938
10.88	1786.6	0.98	3.55	0.85	1732.82	794.87	49.89	0.943
11	1810.0	1.01	2.79	0.86	1785.10	804.92	60.87	0.933
11.1	1829.5	1.00	3.17	0.87	1785.75	764.79	24.14	0.974
11.2	1849.0	0.95	4.08	0.90	1672.83	733.18	52.02	0.938
11.3	1868.5	0.96	3.67	0.89	1755.67	754.79	39.33	0.955
11.4	1888.0	0.92	2.92	0.91	1654.21	621.25	69.01	0.916
11.5	1903.5	0.94	3.19	0.88	1694.88	730.57	42.23	0.950
11.6	1916.4	1.00	2.99	0.88	1853.09	796.81	63.03	0.932
11.7	1929.3	1.14	3.13	0.94	2161.85	934.01	34.62	0.969
11.8	1942.2	0.99	3.66	0.92	1769.01	717.30	36.49	0.959
11.9	1955.1	0.94	3.57	0.91	1722.00	730.16	36.85	0.956
12	1968.0	1.08	2.86	0.86	2007.47	824.00	44.14	0.957
12.32	2009.3	0.90	3.00	0.84	1660.53	666.64	52.66	0.938
12.42	2022.2	0.89	2.99	0.84	1663.24	697.10	66.23	0.919
12.52	2035.1	0.93	2.87	0.82	1796.99	744.87	63.76	0.930
12.62	2048.0	0.92	3.81	0.86	1722.75	750.46	71.79	0.915
12.72	2060.9	0.87	3.36	0.86	1566.76	651.30	44.46	0.944
12.82	2073.8	0.94	3.62	0.88	1786.89	678.21	74.52	0.920
12.94	2089.3	0.89	4.29	0.84	1624.17	668.13	42.12	0.949
13.04	2102.2	0.86	4.19	0.81	1550.77	659.19	42.43	0.947
13.14	2115.1	0.85	3.92	0.83	1544.18	641.94	57.10	0.927
13.24	2128.0	0.86	3.13	0.84	1526.06	668.28	66.04	0.911
13.34	2140.9	0.86	3.76	0.89	1515.81	659.31	36.33	0.952
13.46	2156.3	0.88	3.14	0.91	1580.82	668.81	40.04	0.950
13.66	2182.1	1.07	3.36	0.96	1952.30	866.27	49.97	0.949
13.76	2195.0	0.96	3.61	0.94	1681.13	718.87	40.97	0.952
13.86	2219.7	0.99	3.91	0.92	1730.51	756.71	32.21	0.962

13.96	2245.6	0.91	3.97	0.95	1536.19	695.51	37.54	0.951
14.06	2271.5	0.94	3.38	0.91	1713.11	779.44	38.46	0.955
14.18	2302.6	0.85	3.52	0.90	1515.60	652.71	54.82	0.928
14.3	2333.7	0.87	4.30	0.90	1468.86	630.45	40.40	0.945
14.4	2359.6	1.01	3.57	0.89	1826.89	773.27	53.32	0.941
14.5	2385.5	0.89	3.54	0.90	1429.87	622.89	29.67	0.960
14.6	2411.4	0.90	2.57	0.91	1463.97	641.09	44.48	0.939
14.7	2437.3	0.79	3.58	0.90	1739.68	756.38	36.03	0.960
14.82	2468.4	0.77	4.35	0.92	2060.38	919.34	54.22	0.945
14.92	2494.3	0.91	4.23	0.94	1506.39	632.41	32.22	0.957
15.22	2572.0	0.98	4.06	0.95	1671.67	730.07	43.65	0.947
15.32	2597.9	1.11	3.33	0.93	2012.38	927.25	35.21	0.964
15.42	2623.8	0.99	4.25	0.92	1728.37	792.43	43.39	0.950
15.52	2649.7	0.89	4.53	0.94	1546.88	694.54	42.34	0.946
15.62	2675.6	1.03	3.62	0.92	1820.57	842.82	51.22	0.943
15.72	2701.5	1.00	4.17	0.97	1686.95	765.70	38.55	0.955
15.82	2727.4	1.08	3.32	0.92	1941.04	884.34	44.47	0.954
15.94	2758.5	0.95	4.21	0.97	1557.35	667.43	33.01	0.957
16.04	2778.0	0.95	4.69	0.97	1589.29	672.04	34.84	0.957
16.14	2798.0	1.01	4.60	0.92	1705.41	783.25	45.54	0.947
16.24	2818.0	0.92	5.18	0.93	1438.88	659.68	33.70	0.954
16.34	2838.0	1.01	3.55	0.94	1761.32	776.38	44.62	0.950
16.44	2858.0	1.09	3.25	0.86	1991.57	930.82	37.43	0.963
16.64	2898.0	1.08	3.74	0.83	2005.80	888.93	57.59	0.939
16.74	2918.0	1.01	3.68	0.88	1726.93	739.36	34.35	0.960
16.88	2946.0	1.13	3.35	0.91	2080.67	849.40	66.44	0.935
16.98	2966.0	1.14	3.26	0.94	2101.50	880.40	48.47	0.953
17.08	2986.0	1.42	2.85	0.95	2773.18	1139.40	51.71	0.962
17.18	3006.0	1.10	3.39	0.96	1903.61	746.27	52.56	0.945
17.28	3026.0	1.05	4.45	0.93	1842.45	743.68	55.94	0.942
17.38	3046.0	1.01	2.95	0.86	1779.45	739.13	45.24	0.946
17.48	3066.0	0.95	3.13	0.87	1645.98	669.48	59.00	0.930
17.58	3086.0	0.90	4.37	0.85	1541.95	649.83	58.25	0.924
17.68	3106.0	1.13	3.25	0.82	2154.89	902.13	53.27	0.952
17.8	3130.0	1.00	3.93	0.86	1772.33	661.94	76.61	0.912
17.9	3150.0	1.12	3.29	0.85	2124.99	851.60	87.07	0.917
18.26	3222.0	0.86	3.08	0.77	1601.79	683.47	66.63	0.954
18.36	3242.0	0.89	3.38	0.82	1666.89	692.45	40.70	0.951
18.46	3263.1	0.98	3.00	0.83	1880.16	771.77	52.53	0.944
18.58	3287.5	0.90	2.90	0.84	1663.82	670.10	37.40	0.955
18.68	3307.9	0.99	3.28	0.84	1905.92	799.46	41.84	0.956
18.8	3332.4	0.80	3.44	0.78	1446.12	570.08	38.49	0.947
18.9	3352.8	0.80	3.00	0.73	1472.83	631.47	35.47	0.953

19	3373.2	0.78	3.31	0.71	1478.76	628.87	38.20	0.949
19.1	3393.5	0.69	2.69	0.72	1205.79	488.13	35.19	0.943
19.2	3413.9	0.86	2.29	0.72	1616.34	672.23	35.60	0.956
19.3	3434.3	0.66	2.97	0.70	1187.30	496.31	25.24	0.958
19.4	3454.7	0.66	2.78	0.66	1234.30	524.68	31.27	0.948
19.5	3475.1	0.88	2.63	0.69	1738.29	738.79	42.70	0.951
19.7	3515.8	0.89	2.73	0.73	1792.82	803.85	42.94	0.949
19.8	3536.2	0.75	2.78	0.72	1502.14	659.31	39.86	0.947
19.9	3556.6	0.71	2.87	0.71	1412.32	613.41	32.22	0.955
20	3577.0	0.66	3.26	0.70	1288.80	558.52	32.31	0.949
20.1	3597.4	0.79	2.45	0.70	1636.48	728.41	42.90	0.947
20.2	3617.8	0.79	2.08	0.71	1563.39	677.55	38.72	0.950
20.3	3638.2	0.72	2.66	0.71	1372.78	615.41	29.92	0.956
20.4	3658.5	0.68	3.41	0.67	1295.92	583.66	22.47	0.965
20.5	3678.9	0.70	2.65	0.67	1395.25	605.15	33.21	0.953
20.62	3703.4	0.72	2.31	0.67	1447.78	632.91	32.60	0.955
20.72	3723.8	0.62	1.66	0.64	1236.73	524.39	30.92	0.949
20.82	3744.2	0.78	1.82	0.66	1613.34	736.39	32.65	0.959
20.92	3764.5	0.71	2.22	0.66	1454.32	630.84	27.91	0.962
21.22	3824.0	0.75	2.01	0.64	1577.59	693.16	30.04	0.963
21.32	3844.0	0.62	2.63	0.63	1319.70	541.82	41.80	0.936
21.42	3864.0	0.75	1.89	0.63	1625.25	691.24	53.91	0.936
21.52	3884.0	0.69	1.59	0.63	1499.39	634.91	27.29	0.963
21.62	3904.0	0.72	1.96	0.62	1534.79	648.62	23.93	0.967
21.72	3924.0	0.85	1.83	0.63	1842.65	803.45	49.87	0.944
21.84	3948.0	0.71	1.51	0.57	1545.59	642.13	37.68	0.953
21.94	3968.0	0.59	1.32	0.54	1225.00	497.54	55.88	0.909
22.04	3988.0	0.63	2.07	0.57	1283.61	502.76	29.29	0.956
22.14	4008.0	0.70	1.64	0.59	1454.37	582.35	33.80	0.953
22.24	4028.0	0.81	1.83	0.56	1735.02	752.97	66.52	0.923
22.34	4048.0	0.66	2.51	0.58	1376.54	569.99	48.90	0.930
22.44	4068.0	0.62	2.05	0.59	1300.73	564.57	41.67	0.936

Table 3: Average values and standard deviation of different rock magnetic parameters of MD161/13 and MD161/8.

Magnetic Parameters	Average Value (Mean) MD 13	Std Dev MD 13	Average Value (Mean) MD 8	Std Dev MD 8
$\chi_{LF} \times 10^{-6} \text{ m}^3 \text{ kg}^{-1}$	0.966	0.155	1.185	0.276
$\chi_{fd}\%$	3.235	0.664	5.163	1.037
$\chi_{ARM} \times 10^{-5} \text{ m}^3 \text{ kg}^{-1}$	0.865	0.115	0.849	0.180
$\text{SIRM} \times 10^{-5} \text{ Am}^2 \text{ kg}^{-1}$	1780.432	289.095	1466.577	353.556
$\text{Soft-IRM} \times 10^{-5} \text{ Am}^2 \text{ kg}^{-1}$	754.097	121.166	1236.317	290.369
$\text{Hard-IRM (Hirm)} \times 10^{-5} \text{ Am}^2 \text{ kg}^{-1}$	47.737	13.803	86.800	87.213
S-ratio	0.946	0.014	0.940	0.054
ARM/SIRM	0.020	0.002	0.024	0.004
$\text{SIRM}/\chi \text{ kAm}^{-1}$	18.509	1.450	12.409	1.060